CHALMERS
UNIVERSITY OF TECHNOLOGY

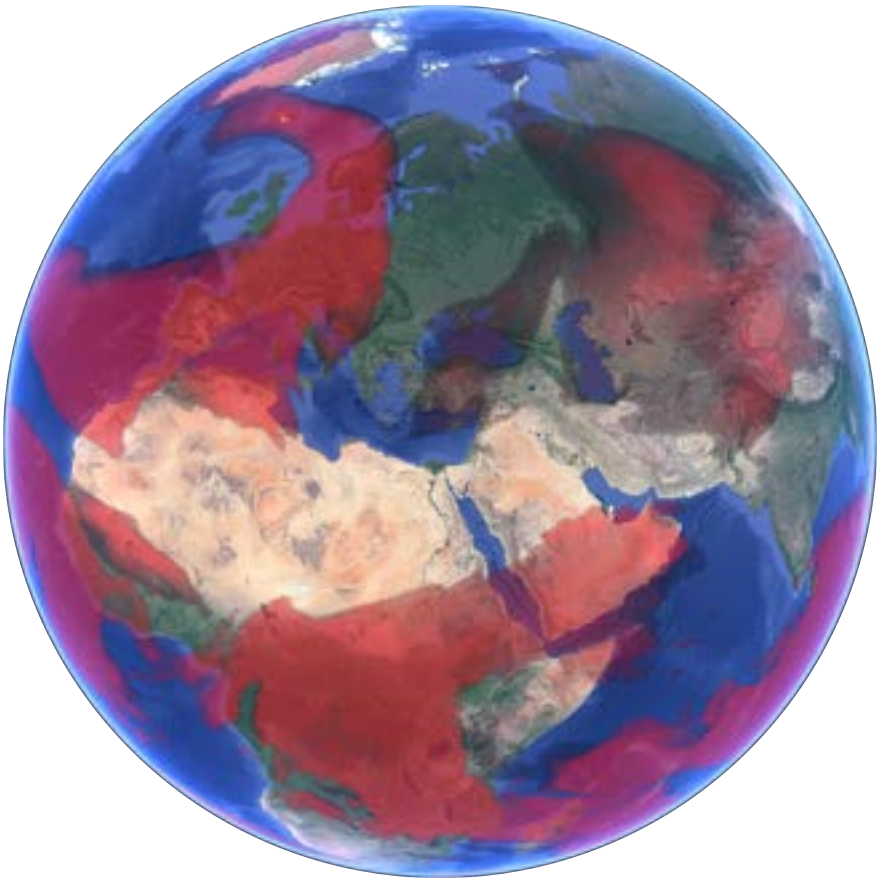

# Strategies to avoid persistent contrail conditions in aviation

## Flight planning strategies for mitigating the climate impact of the aviation industry

Master's thesis in Engineering Mathematics and Computational Science

Johan Gönczi

DEPARTMENT OF SPACE, EARTH AND ENVIRONMENTAL SCIENCE
CHALMERS UNIVERSITY OF TECHNOLOGY
Gothenburg, Sweden 2023
www.chalmers.se

Master's thesis 2023

# Strategies to avoid persistent contrail conditions in aviation

Flight planning strategies for mitigating the climate impact of the aviation industry

Johan Gönczi


CHALMERS
UNIVERSITY OF TECHNOLOGY

Department of Space, Earth and Environmental Science
*Division of Physical Resource Theory*
Chalmers University of Technology
Gothenburg, Sweden 2023

Strategies to avoid persistent contrail conditions in aviation
Flight planning strategies for mitigating the climate impact of the aviation industry
Johan Gönczi



Supervisor: Serguei Tiourine, Jeppesen
Examiner: Daniel Johansson, Department of Space, Earth and Environmental Science

Master's Thesis 2023
Department of Space, Earth and Environmental Science
Division of Physical Resource Theory
Chalmers University of Technology
SE-412 96 Gothenburg
Telephone +46 31 772 1000

Cover: Visualization in Google Earth showing areas where persistent contrail conditions are fulfilled.

Typeset in LaTeX
Printed by Chalmers Reproservice
Gothenburg, Sweden 2023

Strategies to avoid persistent contrail conditions in aviation
Flight planning strategies for mitigating the climate impact of the aviation industry
Johan Gönczi
Department of Space, Earth and Environmental Science
Chalmers University of Technology

# Abstract

This Master thesis discusses strategies to reduce the climate impact of aircraft contrails, which are thin, elongated clouds that can disappear within minutes or endure for several days. Contrail cirrus, i.e., the contrails plus cirrus clouds formed by the enlargement and combination of contrails, are believed to be aviation's main contributor to climate change. Although the exact impact of contrails on the climate is uncertain, it is believed that they contribute to approximately half of the aviation industry's global warming.

The strategies proposed in this thesis mainly consist of creating avoidance areas in airspace that are ice-supersaturated and where the so-called Schmidt-Appleman criterion was fulfilled, which corresponds to airspace where persistent contrails are likely to form. The Alpha shape algorithm was used to construct intricate 2D polygons at each flight level of interest from discrete points in the airspace that fulfilled the conditions. To take the movement of the airspace that fulfilled the contrail conditions into account, the airspace was examined for a few hours and then a temporal threshold was applied to determine where contrails are most likely to form during a flight's duration.

These avoidance areas were then integrated into Jeppesen's industry-leading optimizer as constraints. To compare fuel consumption, flight time, and climate impact, fuel-efficient flight plans were compared with plans that incorporated these avoidance areas. The proposed strategies demonstrate that the climate impact can be significantly reduced with relatively minor increases in flight time and fuel consumption. For some of the notable cases examined, the climate impact was reduced by over 80%, with increased fuel consumption of around 14%. Moreover, there were instances where contrail formation could be significantly or completely reduced with negligible increments in flight duration or fuel consumption.

However, these strategies may not always result in a reduction of the climate impact and the advantages of different strategies depend on atmospheric conditions. Due to increased complexity and potential flight regulation conflicting with the avoidance areas, these strategies may not always return feasible results. Nevertheless, the proposed strategies can be used in parallel and then the preferred flight plan that achieves a satisfactory balance between time, fuel consumption, and climate impact can be selected.

Keywords: Contrails, Aviation, Flight planning, Optimization, Clustering, Alpha shape, SAC.

# Acknowledgements

I am deeply grateful to my supervisor, Sergey Tiourine, and the rest of the team at Jeppesen/Boeing, for proposing such an engaging and interesting topic for my master's thesis. Their guidance and support throughout the entire process have been invaluable, and I couldn't have completed this work without their assistance. I would also like to extend a special thanks to Mats Lindström for his efforts in running all the flight plans on my behalf.

I also extend my gratitude to my examiner, Daniel Johansson, for all of his expertise and help along the way of this thesis. He went above and beyond his duties as an examiner and acted as an additional supervisor, providing valuable feedback and suggestions at every stage of the research. His in-depth understanding of the subject, particularly in relation to climate change, has been essential to ensuring the accuracy and quality of my work.

Additionally, my previous collaboration with Alexander Reusch Eide and Joakim Blomqvist on a related project has played an important role in my understanding of contrail creation. Their expertise has significantly contributed to a smooth start of the thesis.

Johan Gönczi, Gothenburg, June 2023

# List of Acronyms

Below is the list of acronyms that have been used throughout this thesis listed in alphabetical order:

| | |
|---|---|
| AGWP | Absolute Global Warming Potential |
| AIAA | Institute of Aeronautics and Astronautics |
| ECATS | Every Child Accountability & Tracking System |
| ECMWF | European Centre for Medium-Range Weather Forecast |
| EF | Energy Forcing |
| EESI | Environmental and Energy Study Institute |
| ERF | Effective Radiative Forcing |
| FL | Flight Level |
| FRA | Free Route Airspaces |
| GWP | Global warming potential |
| GRIB | General Regularly-distributed Information in Binary form |
| IPCC | Intergovernmental Panel on Climate Change |
| ISA | International Standard Atmosphere |
| ISSR | Ice-Supersaturated Region |
| NetCDF | network Common Data Form |
| NOAA | National Oceanic and Atmospheric Administration |
| NWP | Numerical Weather Prediction |
| RF | Radiative Forcing |
| SAC | Schmidt-Appleman Criterion |
| SID | Standard Instrument Departure |
| STAR | Standard Terminal Arrival Routes |

# Nomenclature

Below is the nomenclature of parameters and variables that have been used throughout this thesis.

## Parameters

| | |
|---|---|
| $EI_{H_2O}$ | Emission index of water vapor |
| $C_p$ | Isobaric specific heat capacity of air |
| $\eta$ | Average propulsion efficiency of a specific jet engine |
| $Q$ | Specific combustion heat |
| $\epsilon$ | Ratio of molar masses of dry air and water vapor |
| $A_{Trop}$ | Surface area of the troposphere |
| $T_{contrail}$ | Life time of a contrail segment |
| $r$ | Efficacy factor |

## Variables

| | |
|---|---|
| $RH_w$ | Relative Humidity with respect to Water |
| $RH_i$ | Relative Humidity with respect to Ice |
| $r_{contr}$ | Critical Humidity threshold for contrail creation |
| $T$ | Temperature |
| $P$ | Pressure |
| $T_{contr}$ | Critical temperature threshold |
| $e_w^{sat}(T)$ | Saturation vapor pressure over water at a given temperature $T$ |
| $e_i^{sat}(T)$ | Saturation vapor pressure over ice at a given temperature $T$ |
| $\mathrm{GWP}_i(T)$ | Global warming potential of gas $i$ for the time horizon $T$ |
| $\mathrm{RF}_i(t)$ | Radiative forcing of gas $i$ at time $t$ |
| $\mathrm{EF}_i(T)$ | Energy forcing of gas $i$ for the time horizon $T$ |

| | |
|---|---|
| $\mathrm{AGWP}_i(T)$ | Absolute global warming potential of gas $i$ for the time horizon $T$ |
| $RF'_{contrail}(t)$ | Local net effect on thermal radiation and solar radiation at time $t$ |
| $L(t)$ | Length of a contrail segment at time $t$ |
| $W(t)$ | Width of a contrail segment at time $t$ |
| $h$ | Altitude in ft |
| $x_i$ | Air distance at time point $i$ |

# Contents

# List of Figures

# List of Tables

# 1
# Introduction

## 1.1 Background

Aircraft can produce thin, elongated white clouds known as aircraft vapor trails (contrails), which may disappear within minutes or endure for several days [1]. If persistent, contrails that begin as linear formations can enlarge and combine with other contrails in regions with heavy air traffic, forming larger cloud formations known as contrail aviation-induced cirrus. However, contrail cirrus will be referred to as contrails in the remaining part of the report. These clouds are believed to be one of the major contributors to climate change caused by aviation [2].

Although the exact impact of contrails on the climate is uncertain, it is believed that they contribute to approximately half of the aviation industry's global warming, as these clouds trap outgoing infrared radiation. The contrail formation in certain areas of the atmosphere is dependent on several factors, among others, humidity, pressure, and temperature, with some locations producing more persistent contrails with longer lifespans. The cost of mitigating the most damaging impact of contrails is projected to be less than US$1 billion per year, with benefits that could exceed 1,000 times that amount [3].

As a result, implementing strategies to reduce the formation of contrails could have a positive impact on the climate, even if it results in increased fuel consumption. Therefore, in the future, Jeppesen would like to offer flight planning services to their customers that take such non-carbon climate impacts into account. In addition, there is a possibility that regulators may introduce a "contrail tax" in the future and thus this thesis may lead to potential economic, as well as ecological benefits.

## 1.2 Aim

The aim of this thesis is to develop a method for assessing the climate impact of flight trajectories that account for the formation of persistent contrails. The proposed approach involves combining weather forecasts for atmospheric conditions and flight trajectories using a custom-built code. To ensure accuracy, interpolation of the airspace parameters in both space and time is necessary. Additionally, an equivalent measure that relates fuel consumption and persistent contrail formation is needed to evaluate the overall climate impact of a trajectory.

This climate measurement approach will be used to analyze several strategies for reducing the climate impact of flight plans. To achieve this, methods for creating 4-dimensional (space and time) structures that satisfy persistent contrail conditions in the airspace will be employed. These structures will be incorporated into Jeppesen's trajectory optimizer as areas to avoid, and the resulting flight paths will be evaluated using the developed climate impact measurement code. Multiple strategies will be assessed to identify a balanced solution between reduced environmental impact, increased flying time, and additional costs from increased fuel consumption.

## 1.3 Objective

The objective of this thesis is to develop strategies and alternative flight paths that achieve a satisfactory balance between reducing the environmental impact, increasing flying time, and increasing fuel consumption.

## 1.4 Limitations and Thesis Focus

The uncertainties surrounding the impact of contrails and their characteristics are great. These characteristics include, among other things, the lifetime, width, and net radiative effect. Therefore, a series of assumptions will be made to be able to give a single measure of the environmental impact. However, this thesis will not try to reduce this uncertainty and instead use and combine different results for these characteristics.

Moreover, the extent of the contrails' impact on the radiative balance and the climate is influenced by the time of day and is greatest during the night. Since flight plans can span multiple time zones, longer flights may occur during both day and night. However, to reduce the complexity of the analysis and utilize a consistent measure throughout the entire flight, only two non-overlapping cases were considered, night or day.

Aviation's impact on the climate stems primarily from two sources: the $CO_2$ emissions from jet fuel and the formation of contrails. Thus, measurements of the climate impact will not consider other emissions, such as $NO_x$.

## 1.5 Societal, Ethical and Ecological aspects

The aim of this thesis is to provide flight planning methods from a climate perspective, which have consequences on both social and ecological systems. Such methods could be utilized in the future to offer customers a wider range of options if they choose to prioritize flights with a lower climate impact. Therefore, any further social, ethical, or ecological aspects do not need to be taken into consideration for this thesis.

# 2
# Theory

## 2.1 Contrails

### 2.1.1 Physical criterias for contrail formation

Condensation trails, also known as contrails, are line shape clouds created by the exhaust from aircraft engines. The thermodynamic theory of contrail formation was formulated by Schmidt [4] and Appleman [5] and thus the theory is named after them. The principle behind the formation of contrail is that when two air masses with varying temperatures and humidity mix, it can result in a supersaturated state that leads to condensation. A common weather phenomenon that is based on this principle is mixing-fog [6].

Condensation of water droplets in the atmosphere typically require the presence of condensation nuclei, which are tiny aerosol particles that allow water vapor to attach and form droplets. Such nuclei are constantly present, however, the burning of kerosene in traditional engines is a major source of particles, particularly soot, which is emitted at a significantly higher number density than that of natural aerosols [7].

Aviation's climate impact is significantly influenced by contrails [2]. However, only persistent contrails have a noticeable impact on the climate, and they form in ice-supersaturated air masses known as ice-supersaturated regions (ISSRs) [6].

### 2.1.2 Contrail model

A slightly modified version of the American Institute of Aeronautics and Astronautics' (AIAA) contrail model described in [8] was employed in this thesis to determine the formation of persistent contrails. The formation of contrails occurs when a combination of the warm engine exhaust gases and the surrounding cold air attains saturation with respect to water, leading to the formation of rapidly freezing liquid drops. The occurrence of contrails is restricted to regions of airspace where the ambient Relative Humidity with respect to Water ($RH_w$) exceeds a critical threshold value of $r_{contr}$ [9]. Furthermore, the contrails could be persistent with a longer lifetime if the Relative Humidity with respect to Ice ($RH_i$) is greater than 100% [10]. Furthermore, parameters were specified to conditions close to cruising altitudes, and altitudes close to the ground are often too warm to create contrails [8]. Thus, simplifying that only altitudes above 25000 ft could fulfill the persistent contrail conditions.

In conclusion, if the atmospheric conditions fulfill all conditions in 2.1, this region of airspace would produce persistent contrails according to the implemented model. These conditions will be referred to as the Smidt-Appleman Criterion (SAC) in the remaining part of the report.

$$\begin{cases} r_{contr} \leq RH_w \\ RH_i \geq 100\% \\ altitude >= 25000\,\text{ft} \end{cases} \tag{2.1}$$

Note that this model will only require the ambient temperature $T$, $RH_w$ and pressure $P$ to determine if the persistent contrail conditions are fulfilled (see section 2.1.2.1 and 2.1.2.2 for further explanation). These variables were provided by the European Centre for Medium-Range Weather Forecasts' (ECMWF) ERA5 database. Further note, that the formulas and parameters in section 2.1.2.1 and 2.1.2.2 were provided by [8] with smaller modifications.

#### 2.1.2.1 Calculating the Critical Humidity Threshold

The estimated critical humidity $r_{contr}$ at a given temperature $T$ (in $°C$) can be calculated as 2.2

$$r_{contr} = \frac{G \cdot (T - T_{contr}) - e_w^{sat}(T_{contr})}{e_w^{sat}(T)}. \tag{2.2}$$

Where $e_w^{sat}(T)$ is the saturation vapor pressure over water at a given temperature $T$. The estimated threshold temperature $T_{contr}$ for contrail formation at liquid saturation is calculated according to 2.3

$$T_{\text{contr}} = -46.46 + 9.43\ln(G - 0.053) + 0.72\ln^2(G - 0.053), \tag{2.3}$$

where the parameter $G$ is defined as 2.4

$$G = \frac{EI_{H_2O} C_p P}{\epsilon Q(1 - \eta)}. \tag{2.4}$$

Where $EI_{H_2O} = 1.25$ is the emission index of water vapor, $C_p = 1004\,\text{JKg}^{-1}\text{K}^{-1}$ is the isobaric specific heat capacity of air, $P$ in Pa is the ambient air pressure. The parameter $\epsilon = 0.6222$ is the ratio of molar masses of dry air and water vapor, $Q = 43 \cdot 10^6\,\text{JKg}^{-1}$ is the specific combustion heat, and $\eta = 0.3$ is the average propulsion efficiency of the jet engine. Note, the value of $r_{contr}$ can be calculated by equations 2.2 - 2.4 and only the pressure $P$ and the temperature $T$ will vary.

#### 2.1.2.2 Calculating the Relative Humidity

The Relative Humidity with respect to Ice $RH_i$ can be calculated by 2.5

$$RH_i = RH_w \frac{e_w^{sat}(T)}{e_i^{sat}(T)}, \tag{2.5}$$

where $e_i^{sat}(T)$ is the saturation vapor pressure of pure water vapor over ice for a given temperature $T\,°\text{C}$. Since the region of interest for this thesis focuses on altitudes

$\sim [25000, 42000]$ ft, the AERK and AERKi approximations (in Pa) were used due to the fact that these approximations are suitable for the temperatures represented in this region [11]. Thus the saturation vapor pressures can be approximated by 2.6

$$\begin{cases} e_w^{sat}(T) = 6.1094e^{17.625T/(243.04+T)} & (AERK) \\ e_i^{sat}(T) = 6.1121e^{22.587T/(273.86+T)} & (AERKi). \end{cases} \tag{2.6}$$

Consequently, the Relative Humidity with respect to Ice can be calculated by 2.7

$$RH_i = RH_w \frac{6.1094e^{17.625T/(243.04+T)}}{6.1121e^{22.587T/(273.86+T)}}. \tag{2.7}$$

## 2.2 Climate impact

### 2.2.1 Radiative forcing

The sun is continuously supplying Earth with energy. Some part of this energy is reflected back into space, while some are directly absorbed by the atmosphere. The remaining part of the energy heats up land and water. This, in turn, causes the temperature on Earth to rise, and the Earth to emit infrared radiation at a level so that, on average the absorbed solar radiation equals the infrared radiation emitted to space [12]. When greenhouse gases are added to the atmosphere, they trap infrared radiation causing an imbalance between incoming solar radiation and outgoing infrared radiation. In order to achieve radiative balance, the temperature on the Earth increases. The disparity in radiative balance that occurs prior to the temperature increase is known as radiative forcing (RF) and is evaluated at the tropopause. It is worth noting that contrails affect both absorbed solar radiation and emitted infrared radiation, as elaborated in section 2.2.3.

Determining a precise value of this unbalance of energy, requires a complex analysis that takes into account a great number of factors, such as polar ice, clouds, and physical characteristics of atmospheric gases. All of these factors add to the complexity of this balancing act and have their own level of uncertainty, making precise measurements challenging. Despite these difficulties, evidence indicates that the Earth is currently receiving more energy than it is emitting, resulting in a positive RF and global warming [13].

### 2.2.2 Global warming potential

The global warming potential (GWP) is a measure of the ability of a greenhouse gas to impact global warming. The scale is relative and compares the effect of the gas $i$ to the effect of an equal amount of carbon dioxide, which makes it easier to compare different gases [14]. The GWP for gas $i$ is defined as 2.8

$$\mathrm{GWP}_i(T) = \frac{\int_0^T \mathrm{RF}_i(t)dt}{\int_0^T \mathrm{RF}_{CO_2}(t)dt} = \frac{AGWP_i(T)}{AGWP_{CO_2}(T)} = \frac{\mathrm{EF}_i(T)}{\mathrm{EF}_{CO_2}(T)}, \tag{2.8}$$

where $T$ is the time horizon and $\mathrm{RF}_i(t)$ is the radiative forcing of gas $i$ at time $t$. The $AGWP_i(T)$ is the Absolute Global Warming Potential of gas $i$ and the $\mathrm{EF}_i(T)$ is the Energy Forcing over the time horizon $T$.

Note that GWP is dependent on several factors, such as the ability to absorb infrared radiation and the longevity of the gas in the atmosphere. Thus if two gases are compared with different characteristics, it may be important to compare different time spans for a better comprehension of the climate impact. For example, assume that gas $i$ has a very high ability to absorb infrared radiation with a very short lifetime in the atmosphere, while gas $j$ has a long lifetime with a lower ability to absorb radiation. In such cases, it is possible that the GWP is higher for gas $i$ for a 20 year perspective, i.e. $\mathrm{GWP}_i(20) > \mathrm{GWP}_j(20)$, while the opposite holds true for a 50 year perspective, i.e. $\mathrm{GWP}_i(50) < \mathrm{GWP}_j(50)$.

Persistent contrails have a relatively short lifespan compared to, for example, $CO_2$ and are formed at high altitudes. Previous research work has demonstrated that individual impact components can have different efficacies, i.e., their effectiveness in inducing changes in surface temperatures. To better compare the impact contributions of these components, Effective Radiative Forcing (ERF) has been proposed as a superior metric. Simulations of climate models have provided estimates of Contrail Cirrus ERF, which is significantly smaller, approximately 65% less than the conventional RF of Contrail Cirrus. However, one should be cautious in drawing any definitive conclusions from this estimation as it is uncertain [15]. As a result, this thesis defines the GWP for contrails as 2.9

$$\mathrm{GWP}_{contrail}(T) = r \cdot \frac{\mathrm{EF}_{contrail}(T)}{\mathrm{EF}_{CO_2}(T)}, \tag{2.9}$$

where $r$ is the so-called efficacy factor and is assumed in this thesis to be 0.35. However, it is important to note that the precise value of this factor remains uncertain. Other credible sources, such as [16], estimate it to be 0.42, which would result in a higher GWP for contrails.

### 2.2.3 Local impact from persistent contrail on the short- and longwave radiation

To begin with, it is important to highlight that the uncertainty surrounding the radiative forcing impact of contrails is significant. Multiple factors come into play when determining the impact of a particular contrail, making it a complex analysis. Nonetheless, the net radiative forcing is a balancing act between the warming and cooling effects of reflection and absorption of incoming shortwave and outgoing longwave radiation. Consequently, the impact of contrails varies with the time of the day, with the greatest impact occurring at night due to the absence of incoming shortwave radiation. As noted in 1.4, flights may cover multiple time zones, leading to flights covering both day and night, and the contrails may persist in the atmosphere for many hours. However, to simplify the analysis and maintain consistency throughout the entire flight, only two non-overlapping cases were considered: night

or day.

Additionally, the impact of contrails is influenced by other factors such as their location and the surrounding environment. The surface below the contrails has a varying albedo, and surfaces with high albedo reflect more sunlight. A higher albedo leads to the contrail having a smaller net impact of solar radiation (i.e. smaller cooling effect), which contributes to, on average larger warming impact of contrails. Therefore, whether the surface below the contrails is water or solid ground can affect the impact. Moreover, the presence of other contrails or clouds above or below a particular contrail can also influence its impact [17].

### 2.2.4 GWP - contrail

Contrails have a local impact on solar radiation and thermal radiation. However, the impact is very uncertain and depends on many properties. We assume that contrails have a local net effect on thermal radiation and solar radiation of $RF'_{contrail}(t)$ $[w/m^2]$. Once again, notice that $RF'_{contrail}(t)$ will differ depending on the time of the day. For example, the reflection of solar radiation, which has a cooling effect only occurs during the day. Thus, $RF'_{contrail}(t)$ is highest during the night since it will not reflect any sunlight.

Furthermore, we assume that the local impact of persistent contrails is constant during its lifetime, i.e. $RF'_{contrail}(t) \equiv RF'_{contrail}$, with a lifetime $T_{contrail}$ $[s]$, i.e. we define the local impact of contrails according to 2.10.

$$RF'_{contrail}(t) = \begin{cases} RF'_{contrail} & t \leq T_{contrail} \\ 0 & t > T_{contrail}. \end{cases} \tag{2.10}$$

Note that this lifetime $T_{contrail}$ is uncertain and estimations vary. According to [18], the typical lifetime of persistent contrails is $T_{contrail} = 3.7 \pm 2.8$ $[h]$. However, on rare occasions, it can have a lifetime of over 24 hours so the distribution is heavily skewed to the right.

To calculate the GWP, we first need to consider the Energy Forcing (EF) of contrails. According to [19], the EF of contrails can be defined as 2.11.

$$\mathrm{EF}_{contrail}(T) = \int_0^T RF'_{contrail}(t) \cdot L(t) \cdot W(t) \mathrm{d}t \tag{2.11}$$

where $L(t)$ $[m]$ is the length of the contrail segment and $W(t)$ $[m]$ is the width of the contrail at time $t$. Note that the width $W(t)$ of contrails is also uncertain and estimations vary. According to [20], contrails has a mean width $W(t) \approx 1000\,\mathrm{m}$. However, due to skewed distribution in lifetime, this width can be much larger [21]. In this case, we assume $L(t)$, $W(t)$ and $RF'_{contrail}(t)$ are constant. Further, note that $\mathrm{RF}_{contrail}(t) = 0$ for $t > T_{contrail}$. Thus, the $\mathrm{EF}_{contrail}(T)$ can be defined as 2.12.

$$\mathrm{EF}_{contrail}(T) = \min(T_{contrail}, T) \cdot RF'_{contrail} \cdot L \cdot W. \tag{2.12}$$

Note that $T_{contrail}$ are estimated to be hours, while the time horizons of interests will be tens of years. Thus, for the time horizons of interest, $\mathrm{EF}_{contrail}(T)$ will be defined as 2.13

$$\mathrm{EF}_{contrail}(T) = T_{contrail} \cdot RF'_{contrail} \cdot L \cdot W. \tag{2.13}$$

Finally, we use the definition 2.9 and equation 2.13 together with the fact that $\mathrm{EF}_{CO_2} = AGWP_{CO_2}(T) \cdot A_{Trop}$ to find the $\mathrm{GWP}_{contrail}(T)$ for the length $L$ [m] persistent contrail created according to 2.14.

$$\mathrm{GWP}_{contrail(L)}(T) = r \cdot \frac{T_{contrail} \cdot RF'_{contrail} \cdot W \cdot L}{\mathrm{A}_{Trop} \cdot AGWP_{CO_2}(T)}, \tag{2.14}$$

where $r = 0.35$ is the efficacy factors, $A_{Trop} \approx 5.121 \times 10^{14}\,\mathrm{m}^2$ is the surface area of the troposphere. The $AGWP_{CO_2}(T)$ can be calculated or available from sources such as the Intergovernmental Panel on Climate Change (IPCC) for the designated time horizon $T$.

## 2.3 Flight regulation

Flight planning involves considering several rules to construct a flight trajectory. Among the most important rules for this thesis are the flight levels, odd-even rule, mid-flight, and departure and arrival regulations.

### 2.3.1 Flight levels

A flight level represents altitude above sea level, measured in 100 ft units according to a standard atmosphere. For instance, FL350 corresponds to an altitude of 35,000 ft above mean sea level. It is important to note that this definition is not a geometric measure. Rather, pressure altitude is defined as the altitude in the International Standard Atmosphere (ISA) at which the atmospheric pressure would be equal to the measured pressure [22]. The National Oceanic and Atmospheric Administration (NOAA) published the following formula 2.15 [23] to convert atmospheric pressure in hPa directly,

$$h = 145366.45 \left[1 - \left(\frac{P}{1013.25}\right)^{0.190284}\right] \tag{2.15}$$

where $h$ is the altitude expressed in ft and $P$ is the pressure in hPa.

Flight levels are utilized to maintain sufficient vertical separation between aircraft, regardless of any natural local variations in atmospheric conditions. The altitude is measured using a pressure altimeter, which measures the ambient air pressure. Flight levels aim to prevent two aircraft from flying at the same altitude, even if their altimeters indicate different altitudes. This is achieved by defining altitudes based on standard air pressure at sea level. All aircraft operating on flight levels are calibrated to this standard setting, irrespective of the actual sea level pressure [24].

### 2.3.2 Odd-even flight levels

Further regulations try to maintain vertical separation between aircraft that are traveling in different directions, in this case, an odd-even regulation. Variations of this rule differ between areas, however, this odd-even rule is also known as the hemispheric rule, as it is used in the eastern and western hemispheres. Under the odd-even flight level rule, air traffic control utilizes a system to keep aircraft flying at different altitudes separated based on their direction of travel. When flying above 29,000 ft, planes that are heading eastbound (0 degrees to 179 degrees) are required to fly at odd-numbered flight levels, such as 31,000, 33,000, and 35,000 ft. Conversely, planes traveling westbound (180 degrees to 359 degrees) must fly at even-numbered flight levels, such as 32,000, 34,000, and 36,000 ft [25].

### 2.3.3 Mid-flight regulation

Traditionally when flying over land, aircraft must fly through predetermined flight paths between specific coordinates in the airspace, called airways. The advances in aero navigation allow aircraft more flexibility in choosing their route in the airspace using so-called Free Route Airspaces (FRA). Flights operating in FRAs will have better options for avoiding contrail formation regions.

### 2.3.4 Departure and Arrival regulation

To ensure safety during takeoff and landing, aircraft must follow specific procedures and paths known as Standard Instrument Departures (SIDs) and Standard Terminal Arrival Routes (STARs). SIDs provide a pre-defined route for aircraft to follow immediately after takeoff, while STARs provide a pre-defined route for aircraft to follow prior to landing. Both SIDs and STARs are designed to help aircraft navigate around other aircraft, obstacles, and terrain, and to ensure safe separation. They also help to optimize the use of airspace and reduce delays by providing standard routes that all aircraft can follow [26].

These regulations can result in seemingly indirect flight paths during landing or departure. For example, aircraft may follow paths that appear to be detours or may even fly in the opposite direction after takeoff.

## 2.4 Optimization

Jeppesen's optimizer calculates a cost-optimal trajectory in space and time variables, taking into account various constraints and regulations. For example in Europe, the flight planning rules are available in the electronic format, the so-called RAD. Additionally, the optimizer considers physical phenomena and atmospheric conditions, such as wind, to create optimal flight plans. While taking all constraints into account, the optimizer identifies a solution that meets requirements while minimizing costs. This presents an excellent opportunity to incorporate additional factors, such as avoiding contrail formation.

## 2.5 Alpha shape

**Definition** [27]: Let $S \subset \mathbb{R}^2$ be a finite set. The $\alpha$-hull of $S$ is the complement of the union of all disks of radius $\alpha$ that contain no points of $S$ in their interior. The $\alpha$-shape of $S$ is a straight-line graph whose vertices are points of $S$ and whose edges connect two points $p, q \in S$ whenever there exists a disk of radius $\alpha$.

Note that the definition is given for a 2D plane. However, this can be extended to $\mathbb{R}^3$ to create volumes. According to Edelsbrunner and Mücke's paper [28], one way to conceptualize an $\alpha$-shape is as follows: imagine a large block of ice cream in $\mathbb{R}^3$ that contains the points in the set $S$ as "hard" chocolate pieces. Using a sphere-shaped spoon with radius $\alpha$, we carve out all parts of the ice cream block that we can reach without hitting the chocolate pieces, creating holes in the inside (i.e., parts not reachable by moving the spoon from the outside). This process results in a body that is bounded by caps, arcs, and points. We then straighten all "round" faces to triangles and line segments. In the 2D case, the spoon would simply be a circle [29]. An example of the 2D alpha shape algorithm is illustrated in Figure 2.1.

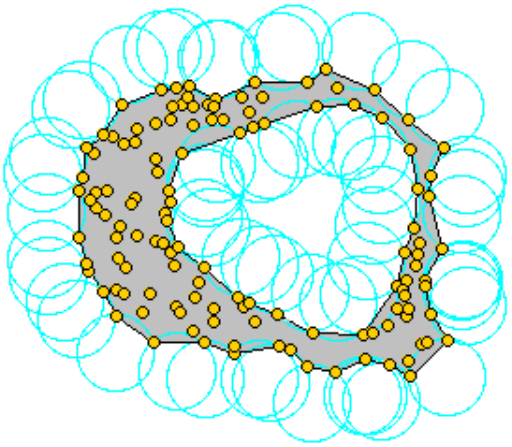

**Figure 2.1:** Example to demonstrate the 2D - alpha shape algorithm [30].

# 3
# Methods

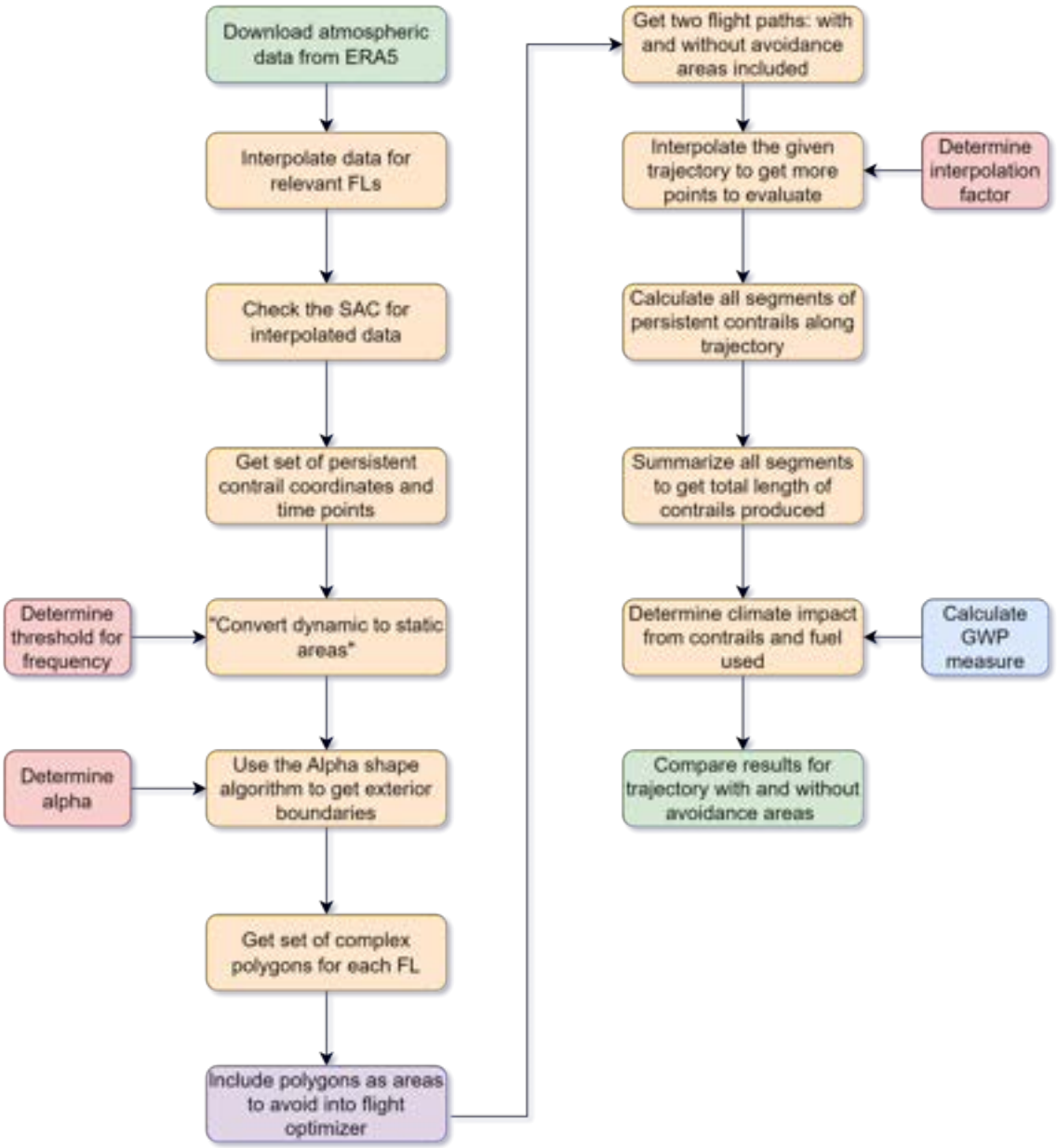


**Figure 3.1:** The thesis work process is visually represented by squares of different colors. The green squares indicate the start and finish points, while the orange squares represent the coding steps. The red squares indicate user-selected parameters, and the purple square represents the step that utilizes Jeppesen's optimizer. Finally, the blue squares represent the use of physical formulas.

## 3.1 Examined routes

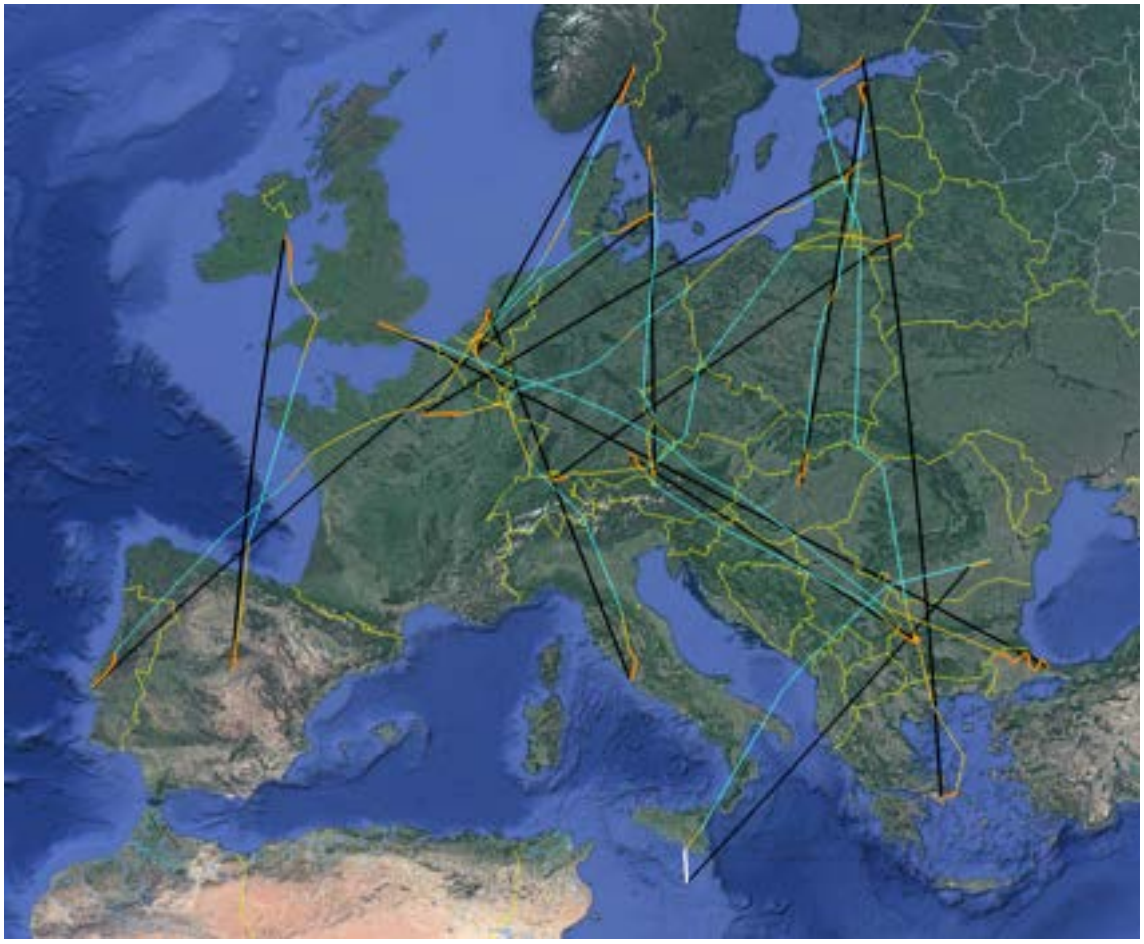

**Figure 3.2:** The European routes that were examined for this thesis. The great circle, which is the shortest path between two airports, is represented by black lines. The SIDs and STARs are shown in dark orange. The corridors in the airspace that the aircraft must follow are depicted by light orange lines. The blue lines depict direct segments in FRAs. It's important to note that this is just one example, and routes may be subject to change due to factors like wind.

Figure 3.2 depicts the European routes examined in this thesis. It should be noted that the destinations were selected randomly, as long as the trajectories covered most parts of Continental Europe. Additionally, note that the examination period was 2022 and as a result, the airspace over Russia and Ukraine was closed due to warfare which could have an impact on certain routes, in particular, LGAV - EFHK (Athens - Helsinki). Table 3.1 contains the departures, destinations, airport codes, and rough estimate of the flight time.

| Departure | | Desitnation | | |
|---|---|---|---|---|
| Code | City | Code | City | Flight time [min] |
| EDDM | Munich | LBSF | Sofia | 88 |
| EGLL | London | LTFM | Istanbul | 192 |
| EHAM | Amsterdam | LIRF | Rome | 108 |
| EKCH | Copenhagen | LPPT | Lisbon | 190 |
| ENGM | Oslo | EBBR | Brussels | 90 |
| ESGG | Landvetter | LOWS | Salzburg | 93 |
| EYVI | Vilnius | LSZH | Zurich | 128 |
| LEMD | Madrid | EIDW | Dublin | 115 |
| LFPG | Paris | EVRA | Riga | 128 |
| LGAV | Athens | EFHK | Helsinki | 207 |
| LHBP | Budapest | EETN | Tallin | 110 |
| LROP | Bucharest | LMML | Malta | 132 |

**Table 3.1:** The European flights with departures and destinations. Note that the flight time is a rough estimate from one typical route and may change due to, for example, wind.

## 3.2 Meteorology data

According to the persistent contrail model (see section 2.1.2), temperature, humidity, and pressure are required to determine if the SAC was fulfilled. These necessary atmospheric parameters were provided by the European Centre for Medium-Range Weather Forecasts' (ECMWF) ERA5 database. ERA5 is the fifth-generation ECMWF reanalysis for global climate and weather. It combines model data and observations from around the world using the laws of physics to create a globally complete and consistent data set. The resulting data is in the form of pressure levels expressed in hPa and a latitude and longitude grid with a resolution of 0.25 degrees. The data have a 1-hour temporal resolution, resulting in a three-dimensional grid with coordinates of (longitude, latitude, pressure) and time [31]. The user can select specific areas and pressure levels of interest and download the data in a GRIB or NetCDF format. In this case, the GRIB format was selected.

## 3.3 Determine the airspace to avoid

The initial step involved selecting flight levels of interest where to potentially avoid airspace that met persistent contrail conditions. Next, atmospheric data were interpolated for these flight levels. The SAC was then applied to determine if a specific point met the persistent contrail criteria for all latitudes, longitudes, flight levels, and time points. In addition, the movement of airspace that met contrail conditions was considered by examining multiple time points. For each flight level, 2D polygons were generated from the persistent contrail points using the alpha shape algorithm. These polygons were subsequently formatted and input into the optimizer as areas to avoid.

### 3.3.1 Selecting flight levels of interest

The determination of flight levels to potentially create avoidance areas depends on three primary factors. Firstly, since aircraft spend the majority of their flight time at cruising altitudes, typically around 35,000 to 40,000 ft, creating areas to avoid far from this range will require more computational time but most likely not impact the optimization. Additionally, the upper limit of the airspace of interest mainly depends on an aircraft's ability to fly at high altitudes, and most commercial planes cannot fly far above 42,000 ft.

Due to regulations, given a specific airport, a selection of specific procedures must be carried out (see section 2.3.4 for further explanation). Thus the avoidance areas might conflict with the procedures, rendering the flight plan infeasible. Consequently, different lower limits for the altitude were examined.

### 3.3.2 Interpolate atmospheric data for flight levels of interest

Interpolation of the data to the flight levels of interest was required. This was done by first converting the desired altitudes to pressure levels using the formula 2.15. The atmospheric dataset was downloaded and saved in a variable ds, using the Python library, Xarray, in combination with the engine, cfgrib. Subsequently, the data were interpolated for the designated pressure levels, as illustrated in the following example:

```
import xarray as xr

# ds is the variable containing the weather data.
# Adr_to_grib is the adress to the downloaded and
# stored atmospheric data (GRIB file).
ds = xr.load_dataset(Adr_to_grib, engine='cfgrib')

# altitude_array is an an array of altitudes in ft,
# for example [25000, 26000, ... , 42000]
# alt_to_pressure_in_hpa() is a function that
# converts altitude to pressure level
isobar_array = alt_to_pressure_in_hpa(altitude_array)

# Interpolate the data for the specific pressure levels.
# isobaricInhPa is the name of the parameter for the pressure.
# The interpolation is linear as a deafult
ds_interpolated = ds.interp(isobaricInhPa = isobar_array)
```

Note that the function **ds.interp()** "performs univariate or multivariate interpolation of a DataArray onto new coordinates using Scipy's interpolation routines. If interpolating along an existing dimension, scipy.interpolate.interp1d is called. When interpolating along multiple existing dimensions, an attempt is made to decompose the interpolation into multiple 1-dimensional interpolations. If this is possible,

scipy.interpolate.interp1d is called. Otherwise, scipy.interpolate.interpn() is called" [32]. In this case, the scipy.interpolate.interpn() was called and is using as a default a linear interpolation. Further note that the "interpolant is constructed by triangulating the input data together with the convex hull, and on each triangle performing linear barycentric interpolation" [33].

### 3.3.3 Determine if the persistent contrail conditions are fulfilled

After interpolating the data, the next step was to determine whether the atmospheric conditions met the SAC for all flight levels of interest and time points. Each time point and coordinate in the interpolated dataset was examined, and if the conditions were met, it was assigned a value of 1 and 0 otherwise. This resulted in matrices of zeros and ones for all time points and flight levels, indicating whether the conditions were fulfilled or not.

### 3.3.4 Take movement of airspace into consideration

Due to the fact that the input for the optimizer was static areas for each flight level of interest, the movement of airspace that met contrail conditions was considered by examining multiple time points. For instance, if a flight begins at 2:00 PM and lasts for 5 hours, the airspace that satisfies persistent contrail conditions might shift during the flight's duration. To address this, the 5-hour period was examined and the number of hours in which the given coordinates satisfy the conditions was summarized. Then a threshold was applied to only cluster points that were fulfilled more or equal to this threshold. This is demonstrated in the following simple example 3.3:

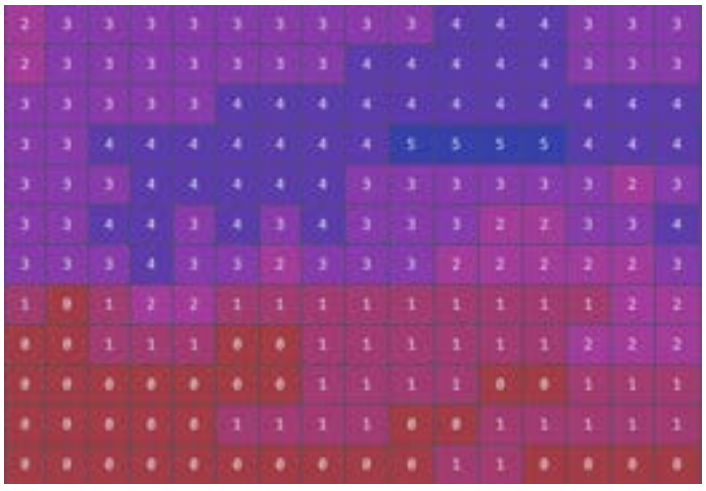

**Figure 3.3:** Example where each cell in the matrix corresponds to the number of times where these coordinates fulfilled the persistent contrail conditions during the 5-hour period. Note that this is a very small portion of Europe's airspace.

It should be noted that a high selected threshold will result in smaller deviations from the cost-effective routes but with a higher likelihood to produce persistent con-

trails during the flight. Conversely, a smaller threshold will lead to more significant deviations but a reduced probability of contrail formation. Consequently, different thresholds were evaluated to find a suitable balance for the deviations from the cost-effective routes.

### 3.3.5 Cluster the persistent contrail points for flight levels of interest

Given the examination of several time points and selected threshold, a clustering was conducted. For each flight level of interest, the 2D alpha shape algorithm was used to create exterior boundaries of the airspace that met the persistent contrail conditions more or equal to the selected threshold. This is demonstrated in the following Figure 3.4.

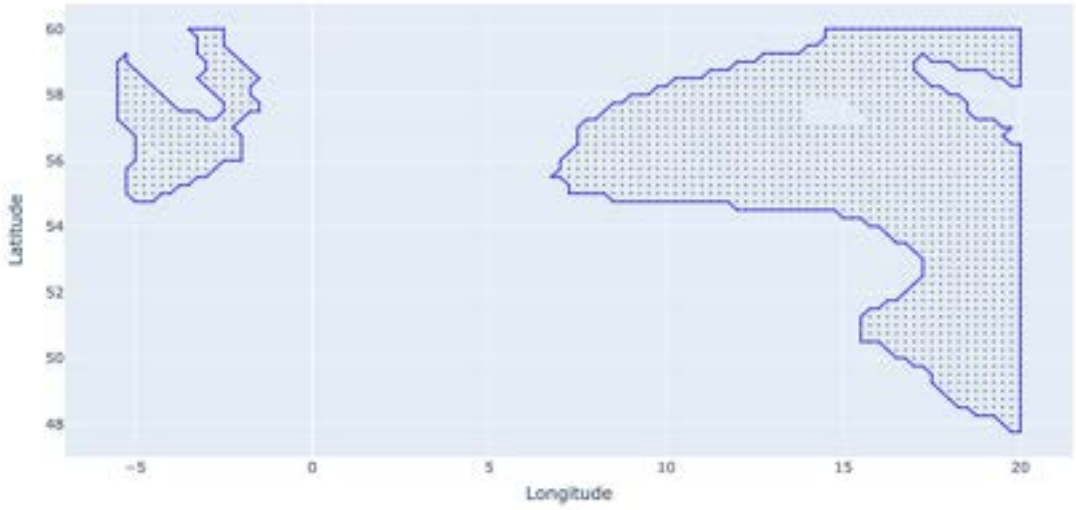


**Figure 3.4:** The figure depicts one example for one altitude of 37 000 ft across a portion of Europe's airspace. The 2D alpha shape algorithm with $\alpha = 4.5$ generated the light blue lines, which represent the exterior boundaries of the clustering. The black dots represent the coordinates that met the persistent contrail conditions for at least four out of five time points. The dataset included atmospheric parameters for latitudes and longitudes ranging from 40 to 60 degrees and -10 to 20 degrees, respectively. Note that this example is separate from the example illustrated in Figure 3.3.

For each flight level of interest, the algorithm can produce a variety of complex polygons, as illustrated in Figure 3.4. To create avoid volumes for the aircraft in the airspace, the volume is assumed to extend vertically by $\pm 5$ flight levels from the level where the clustering was performed. It should be noted that each cruising altitude is separated by 10 flight levels. Consequently, the generated volumes will not overlap. Finally, these volumes were converted into avoid volumes in the airspace, which were then utilized in flight planning optimization to ensure avoidance.

## 3.4 Evaluate the environmental impact of trajectory

To evaluate the environmental impact of a specific trajectory, multiple steps were required. First of all, the optimizer generates a trajectory with a sparse amount of time points and corresponding coordinates along the trajectory. In order to extend the number of points available for examination, an interpolation was conducted. Next, atmospheric conditions were interpolated for the set of interpolated points along the trajectory. Each point in space and time was then examined to determine if it satisfied the persistent contrail conditions. Finally, the resulting contrail segments were summarized to determine the total length of contrails produced by the trajectory.

### 3.4.1 Interpolation of the given trajectory

The trajectory generated by the optimizer contains a sparse amount of points, so spatial and temporal interpolation was performed to increase the number of points for evaluation. A linear interpolation was then conducted for all dimensions, including latitude, longitude, altitude, air distance, and time, and a preferred multiple of the interpolated points was examined. A higher multiple is preferred to ensure the accuracy of each contrail segment's length (see section 3.4.3 for further details).

### 3.4.2 Interpolation of the atmospheric conditions in space and time

From the interpolated set of points in space and time along the trajectory, an interpolation of the atmospheric conditions for these points was performed. In this case, to reduce the computational time, a subset of the data was first extracted. For each point in space and time along the trajectory, the data containing atmospheric conditions surrounding this point, i.e. a 4-dimensional box (space and time) was extracted. Following this, a linear interpolation was performed for each point with the respective 4d box to calculate the atmospheric conditions.

### 3.4.3 Calculate the length of contrail segment

Given the atmospheric conditions for each point along the interpolated trajectory, the conditions for persistent contrails were examined. Then, given that a point fulfilled the conditions, it is assumed that the segment between the middle of the two surrounding points fulfilled the conditions. Thus, the segment length of a persistent contrail was calculated with the following formula 3.1:

$$L_{contrail}(i) = \frac{x_{i+1} - x_i}{2} + \frac{x_i - x_{i-1}}{2} = \frac{x_{i+1} - x_{i-1}}{2}, \tag{3.1}$$

where $L_{contrail}(i)$ is the segment length given that point $i$ fulfilled the persistent contrail conditions and $x_{i+1}$, $x_i$ and $x_{i-1}$ are the air distance at time point $i+1$, $i$ and $i-1$, respectively. Note that the formula ignores the endpoints, i.e. the takeoff

and landing. However, since the endpoints will be very close to the ground where the contrail conditions are highly unlikely to be fulfilled due to the high temperature close to the ground, it will most likely not affect the accuracy.

A greater number of interpolated points for the trajectory would improve the accuracy of the contrail segments since this formula assumes that the airspace between the middle of the surrounding points met the contrail conditions. Thereafter, all these segments were summarized, which in turn resulted in the total length of persistent contrails produced from the given trajectory. It is worth noting that the resulting length remained relatively stable, with only small deviations, despite variations in the number of interpolated points. Finally, this total length $L$ was inserted in the constructed formula 2.14 to calculate the environmental impact of the persistent contrails produced by the given flight.

## 3.5 Forcing the plane to cruise at higher altitudes

By incorporating a multitude of intricate polygons for each flight level, the optimization complexity increases significantly. This, in turn, results in a longer computation time for the optimizer. Moreover, higher altitudes appear to have fewer contrail areas (see 4.1 for further details). Additionally, if the avoidance areas interfere with the SIDs and STARs procedures described in 2.3.4 during takeoff or landing, the flight plan may be infeasible for those specific atmospheric conditions and routes. As a result, an alternative strategy was explored. This approach involves creating avoidance areas only for higher altitudes, such as above $34,000\,\text{ft}$, and then forcing the aircraft to cruise at those altitudes. However, it should be noted that the location and timing of when the aircraft begins cruising appeared to be somewhat ambiguous.

# 4

# Results

## 4.1 Avoidance Areas

Figure 4.1 was created using the methodology described in 3.3 to determine the airspace to avoid for the particular atmospheric conditions. These avoidance areas are applicable for the date range of 01/10/2022 between 13:00 - 15:00. It should be noted that this is a 2-hour span. However, the data contain three time points: 13:00, 14:00, and 15:00. For the other cases, see Appendix A.1.

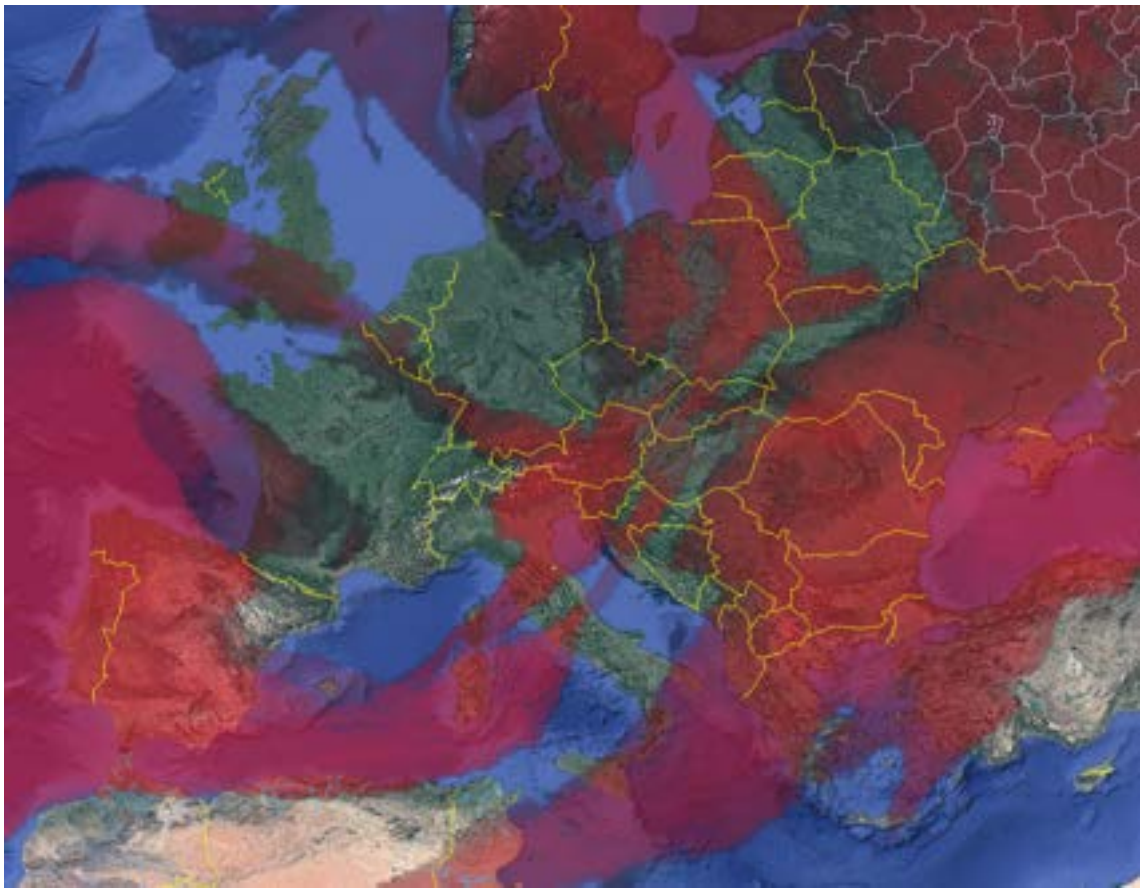

**Figure 4.1:** Europe's airspace is marked with gradient shades of red to indicate the avoidance areas. These areas are formed through the clustering of a 2 out of 3 temporal threshold with $\alpha = 4.5$ in the alpha shape clustering method described in 3.3. The atmospheric conditions for the avoidance areas are applicable for the date range of 01/10/2022 between 13:00 - 15:00.

Note that the avoidance areas were generated by stacking multiple intricate 2D polygons of the exterior boundaries created by the Alpha shape algorithm for altitudes ranging from 25,000 ft to 42,000 ft with 1,000 ft increments. The 2D polygons will extend vertically $\pm 5$ flight levels ($\sim 300$ m in total) from the level where the clustering was performed, creating volumes as the input to the optimizer.

Furthermore, it should be noted that even if the large clusters may seem to be "solid", there could exist feasible paths over, under, or within the avoidance areas. For further detail, see example 3.4. The different gradients of red represent the altitude where the 2D clustering was performed and lower altitudes are depicted with darker colors. The darker colors, in this particular case, can be seen around the outer parts of the larger clusters. In addition, the atmospheric data used to create these avoid areas cover a range of latitudes and longitudes from 20 to 80 degrees and from $-20$ to 50 degrees, respectively. Consequently, as seen in the top-left corner of the map, some areas may be cropped. However, the analyzed flights fall within these latitude and longitude ranges for the atmospheric data.

The avoidance areas shown in 4.1 and Appendix A.1 visually demonstrate that areas that fulfill the persistent contrail conditions tend to form large clusters, forming cloud-like structures in the airspace. Moreover, comparing avoidance areas during the nighttime (02:00-04:00) and daytime (13:00-15:00) on a single day, it becomes apparent that these areas are not static but are constantly moving and transforming. In a prior project conducted before this thesis, a clear correlation was observed between the wind and the movement of contrail areas.

### 4.1.1 Avoidance Areas - Temporal threshold

As explained in 3.3.4, the size of the avoidance areas will be determined by the chosen temporal threshold. The temporal threshold can be thought of as how much of the core of the clusters that will be considered during the examined time span. A higher temporal threshold will result in smaller avoidance areas but with a greater likelihood of meeting the conditions for persistent contrails throughout the entire flight. Figure 4.2 illustrates the same weather conditions for two different cases with varying temporal thresholds.

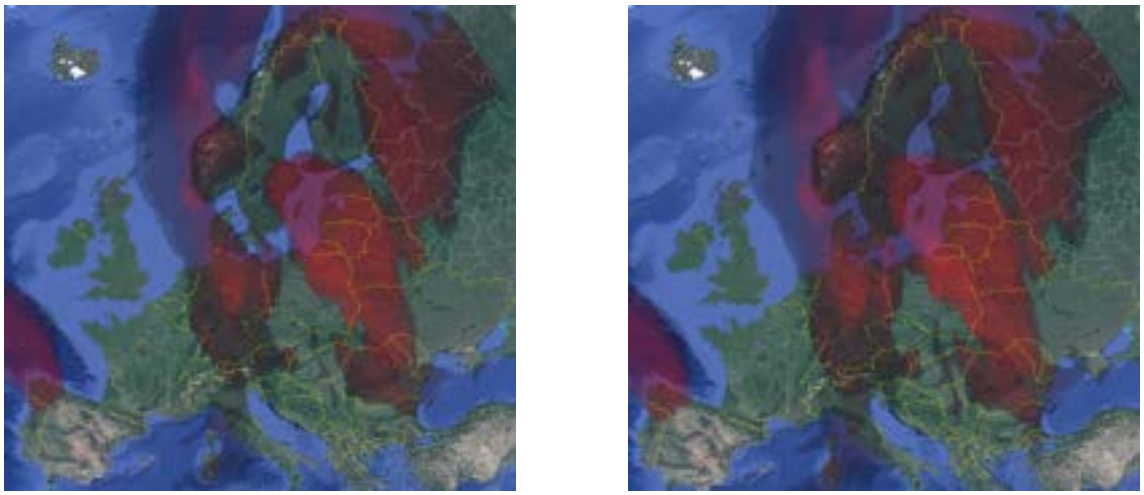

**(a)** Temporal threshold: 2 out of 3. **(b)** Temporal threshold: 1 out of 3.

**Figure 4.2:** Europe's airspace is marked with gradient shades of red to indicate the avoidance areas. These areas are formed through two different cases for the temporal threshold and with $\alpha = 4.5$ in the alpha shape clustering method. The atmospheric conditions for the avoidance areas are applicable for the date range of 01/7/2022 between 02:00 - 04:00 and FL340 - FL420.

Notice in Figure 4.2 that the clusters are larger with a lower temporal threshold. Notably, the separation between the two distinct clusters above the southern part of Sweden's airspace disappears with the lower threshold. Under such conditions, with very large clusters surrounding an airport, it is unlikely that the optimizer would find a flight plan using some of the strategies presented in this thesis, as explained in more detail in 4.2.

### 4.1.2 Avoidance Areas - Different Altitude Ranges

There are different advantages to creating avoidance areas for different altitude ranges, which will be further explained in 4.2. To visually demonstrate the dependency of altitude ranges, see Figure 4.3.

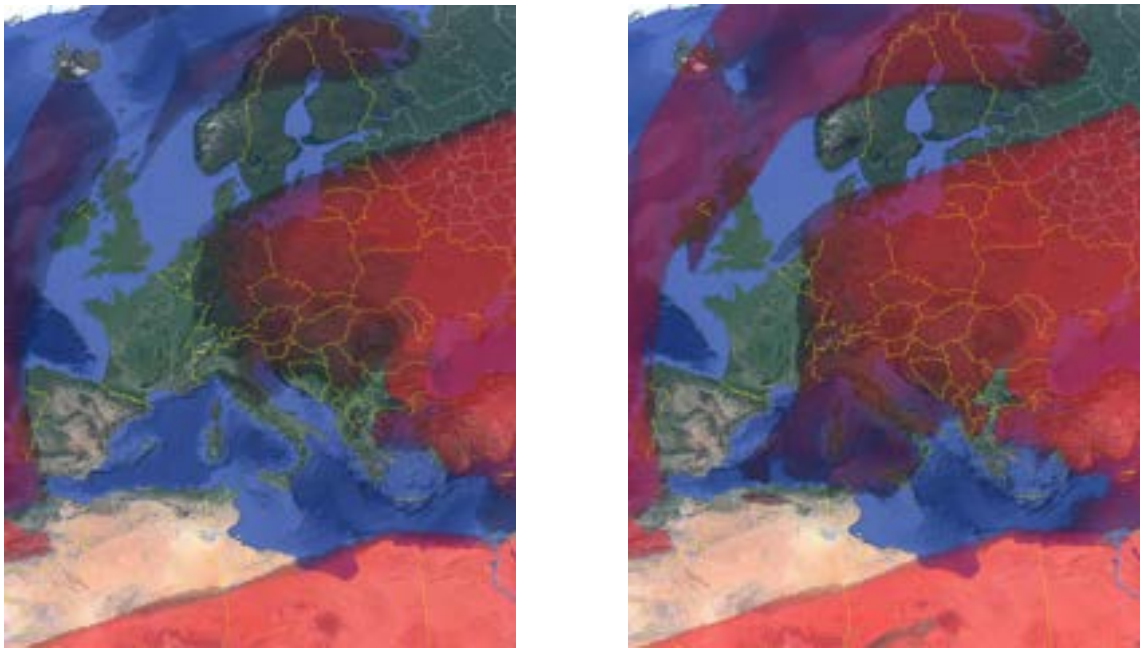

**(a)** Altitude range: 34,000 to 42,000 ft.

**(b)** Altitude range: 25,000 to 42,000 ft.

**Figure 4.3:** Europe's airspace is marked with gradient shades of red to indicate the avoidance areas. These areas are formed through two different cases for the altitude ranges and with a temporal threshold of 2 out of 3 and $\alpha = 4.5$ in the alpha shape clustering method. The atmospheric conditions for the avoidance areas are applicable for the date range of 01/4/2022 between 02:00 - 04:00.

Observe from Figure 4.3 that the clusters are notably larger in the altitude range starting from 25,000 ft in Figure 4.3b than in 4.3a, particularly north of the UK and south of Italy. Therefore, for this atmospheric data, a significant portion of Europe's airspace between 25,000 and 34,000 ft satisfied the contrail conditions.

## 4.2 Flight Optimization - With and Without Avoidance Areas

The avoidance areas, which can be observed in 4.1 and A.1, were transformed and utilized as constraints in Jeppesen's optimizer. A comparison was made between the flight's duration, fuel usage, persistent contrail creation, and total climate impact (persistent contrails and fuel) when the constraints were applied and not. These comparisons were carried out for four days selected randomly, covering the four seasons and with departures during the night (02:00) and day (13:00).

For the following results, the $\mathrm{EF}_{contrail}(100)$ was assumed to be $2 \cdot 10^8\,\mathrm{J/m}$ and $8 \cdot 10^8\,\mathrm{J/m}$ during the day and night, respectively. Note that these assumptions align with estimations from the third ECATS Conference [19] and European Geosciences Union [34]. However, once again, these estimations are uncertain and these

results should be regarded as illustrative potentials of the climate impacts. Furthermore, taking an efficacy factor of $r = 0.35$ into account, the resulting GWP values for contrails were 48.45 and 193.78 CO2 equivalents per kilometer of persistent contrail created during the day and night, respectively. According to the Environmental and Energy Study Institute (EESI) [35], by neglecting any other gases than $CO_2$ in the combustion, 1 kg of jet fuel is equivalent to 3.16 kg of $CO_2$.

For consistency, all simulations use a Boeing 737-800 aircraft with a CFM56-7B24 engine and fixed payload. However, the optimizer may not return results for some routes that include avoidance areas. This may occur due to two main possible causes. Firstly, the avoidance areas may interfere with the SID and STAR procedures during takeoff or landing, resulting in an infeasible flight plan. Secondly, the high complexity introduced by the avoidance areas may prevent the optimizer from finding an optimal feasible solution within the allowed computational time.

Different temporal thresholds were examined during this thesis. When a temporal threshold of 1 out of 3 hours was applied, the avoidance areas were quite large, and separate clusters joined, as seen in Figure 4.2 and in turn, resulted in very few completed and feasible optimized flights. Consequently, a temporal threshold of 2 out of 3 hours is used for these results. However, one case with a temporal threshold of 1 out of 3 hours is included in Appendix A.2.

Moreover, it should be noted that the alpha shape algorithm requires more than a singular point in the horizontal plane to define an area. As a result, there may be isolated points within the airspace where persistent contrail conditions are met that are not covered by the avoidance areas. Additionally, the use of a temporal threshold greater than one (as explained in Section 3.3.4) means that the avoidance areas only represent where contrail conditions are likely to occur. Consequently, it is possible for an aircraft to still create persistent contrails even if it does not fly within the avoidance areas.

Finally, as mentioned in 3.4.3, the calculated total length of persistent contrails may vary depending on the number of interpolated points used for the trajectory. However, the differences observed were small, with deviations mostly below $\sim 2\%$ when using different interpolation factors. To maintain consistency, all outcomes utilized an interpolation factor of 2, which doubles the number of points along the trajectory.

### 4.2.1 Flight Optimization - Whole Airspace

To begin with, cases with avoidance areas ranging from 25,000 ft to 42,000 ft were examined, two of which are included. However, this strategy may result in few feasible and optimized flight plans from the optimizer, depending on the atmospheric conditions. In this case, the most likely explanation for the limited number of flight plans is that the avoidance areas interfere with the takeoff and landing procedures outlined in the SID and STAR, resulting in infeasible flight plans.

| Summer night time - Whole Airspace | | | | | |
|---|---|---|---|---|---|
| Departure | Destination | Change [%] | | | |
| | | Contrails | Time | Fuel | Climate impact |
| EDDM | LBSF | -0.11 | 0.54 | 1.61 | 0.98 |
| EGLL | LTFM | -100 | -0.03 | 0.19 | -54.14 |
| EHAM | LIRF | NaN | NaN | NaN | NaN |
| EKCH | LPPT | NaN | NaN | NaN | NaN |
| ENGM | EBBR | NaN | NaN | NaN | NaN |
| ESGG | LOWS | -43.06 | 6.66 | 7.0 | -30.97 |
| EYVI | LSZH | NaN | NaN | NaN | NaN |
| LEMD | EIDW | 0 | 0 | 0 | 0 |
| LFPG | EVRA | NaN | NaN | NaN | NaN |
| LGAV | EFHK | NaN | NaN | NaN | NaN |
| LHBP | EETN | NaN | NaN | NaN | NaN |
| LROP | LMML | 0 | 0 | 0 | 0 |

**Table 4.1:** The percentage difference between flights that include avoidance areas and those that don't. A positive value represents an increase when avoidance areas are taken into account. These are the outcomes obtained for a summer night with a departure time of 02:00 - 01/07/2022. The avoidance areas can be seen in A.6.

Table 4.1 demonstrates that this strategy may result in a limited number of executed flight plans. Nevertheless, for two of the routes, the climate impact was significantly reduced with only a relatively small increase in fuel consumption. The EGLL-LTFM route, in particular, showed a total reduction of persistent contrail formation without a notable increase in fuel consumption. Moreover, the deviation from the initial flight plan was relatively minor compared to the scenario with avoidance areas, as illustrated in Figure 4.4.

**Figure 4.4:** One example highlighted from the results with avoidance areas for the whole altitude range. The flight plan from EGLL to LFTM that includes avoidance areas results in a rerouting that flies south across Germany.

The illustration in Figure 4.4 demonstrates that even minor deviations from the original fuel-efficient flight plan can significantly reduce persistent contrail formation. The vertical profiles can be seen in A.3.1. It is worth noting that in this particular case, the rerouting primarily involves changes in altitude, with only minor adjustments in the latitudinal and longitudinal plane.

The next case examined is a fall night. The results can be seen in Table 4.2 with respective avoidance areas that can be seen in A.7. Note that from a visual inspection, the coverage of avoidance areas is greater compared to the previous case in Figure A.6.

| Fall Night time - Whole Airspace | | | | | |
|---|---|---|---|---|---|
| Departure | Destination | Change [%] | | | |
| | | Contrail | Time | Fuel | Climate impact |
| EDDM | LBSF | NaN | NaN | NaN | NaN |
| EGLL | LTFM | NaN | NaN | NaN | NaN |
| EHAM | LIRF | -100 | 7.11 | 13.72 | -89.34 |
| EKCH | LPPT | NaN | NaN | NaN | NaN |
| ENGM | EBBR | NaN | NaN | NaN | NaN |
| ESGG | LOWS | NaN | NaN | NaN | NaN |
| EYVI | LSZH | -52.61 | 3.09 | 6.64 | -36.15 |
| LEMD | EIDW | -100 | 9.22 | 19.86 | -86.78 |
| LFPG | EVRA | NaN | NaN | NaN | NaN |
| LGAV | EFHK | NaN | NaN | NaN | NaN |
| LHBP | EETN | -79.11 | 2.45 | 5.57 | -44.13 |
| LROP | LMML | NaN | NaN | NaN | NaN |

**Table 4.2:** The percentage difference between flights that include avoidance areas and those that don't. A positive value represents an increase when avoidance areas are taken into account. These are the outcomes obtained for a fall night with a departure time of 02:00 - 01/10/2022. The avoidance areas can be seen in A.7.

All optimized and feasible outcomes with avoidance areas included resulted in a significant reduction in contrail creation, as can be in Table 4.2. Consequently, for this particular case, all deviating flight plans from the initial fuel-efficient flight plans resulted in a reduction in climate impact, even when the fuel consumption increased.

### 4.2.2 Flight Optimization - Forcing the aircraft to cruise at higher altitudes

As mentioned in 3.5, the complexity for the optimization increases significantly when avoidance areas are included. In addition, if the avoidance areas interfere with the SIDs and STARs procedures described in 2.3.4 during takeoff or landing, the flight plan will be infeasible. Finally, it could be beneficial to fly at higher altitudes where contrails are less likely to form. Thus another strategy was examined, to create avoidance areas from $34,000\,\text{ft}$ and force the aircraft to cruise above that altitude for the whole flight except during take-off and landing. However, the precise timing for when the aircraft needs to begin cruising seems to be somewhat ambiguous. In addition, the optimizer would not take into account any areas below $34,000\,\text{ft}$ where the airspace may fulfill the SAC, and thus the results may on average be worse compared to when the whole range above $25,000\,\text{ft}$ were taken into consideration. Furthermore, this constraint was used for the fuel-efficient flight plans as well. However, since the optimal cruising altitudes will (almost always) be above this constraint, it will not affect these fuel-efficient flight plans.

Keep in mind that the climate impact from persistent contrails is assumed to be

roughly four times as great during the night compared to the day. Consequently, the same reduction of contrail creation will result in a greater reduction in climate impact for the night cases.

#### 4.2.2.1 Flight Optimization - Winter

Tables 4.3 and 4.4 show the results for a winter day (01/01/2022) during day and night time, respectively. The aircraft are forced to cruise above 34,000 ft. The avoidance areas are illustrated in Figures A.1 and A.2.

| **Winter Day time - Forcing higher altitudes** | | | | | |
|---|---|---|---|---|---|
| Departure | Destination | **Change [%]** | | | |
| | | Contrails | Time | Fuel | Climate impact |
| EDDM | LBSF | -84.92 | 0.66 | 2.46 | -62.42 |
| EGLL | LTFM | NaN | NaN | NaN | NaN |
| EHAM | LIRF | NaN | NaN | NaN | NaN |
| EKCH | LPPT | NaN | NaN | NaN | NaN |
| ENGM | EBBR | NaN | NaN | NaN | NaN |
| ESGG | LOWS | 1.21 | 0.95 | 3.25 | 1.64 |
| EYVI | LSZH | NaN | NaN | NaN | NaN |
| LEMD | EIDW | NaN | NaN | NaN | NaN |
| LFPG | EVRA | NaN | NaN | NaN | NaN |
| LGAV | EFHK | 0 | 0 | 0 | 0 |
| LHBP | EETN | -80.59 | 0.61 | 2.36 | -55.39 |
| LROP | LMML | 0 | 0 | 0 | 0 |

**Table 4.3:** The percentage difference between flights that include avoidance areas and those that don't. A positive value represents an increase when avoidance areas are taken into account. These are the outcomes obtained for a winter day with a departure time of 13:00 - 01/01/2022. The avoidance areas range from 34,000 ft to 42,000 ft and the aircraft is forced to cruise at a minimum of 34,000 ft. If no solution was obtained by the optimizer with the avoidance areas included, the values are NaN. The avoidance areas can be seen in A.1.

The results presented in Table 4.3 indicate that out of five completed flight plans, two of them did not require any changes to the initial optimized fuel-efficient route. Notably, the LROP-LMML route did not generate any contrails in the initial route and therefore did not necessitate any deviations when avoidance areas were included. On the other hand, the LGAV-EFHK route produced a relatively small amount of persistent contrails, totaling 46.51 km, without any alterations to the flight plan. The two possible explanations for this could be that the temporal threshold was greater than 1 or that the contrails were formed during the ascent or descent to/from the cruising altitude, where avoidance areas were not applied. The EDDM-LBSF and LHBP-EETN routes demonstrated a considerable reduction in contrail formation with minor increases in fuel consumption, which in turn, resulted in a significant reduction in climate impact. The ESGG-LOWS route resulted in a slight increase in

both contrail formation and fuel consumption, in such cases the initial route should always be selected.

| **Winter Night time - Forcing higher altitudes** | | | | | |
|---|---|---|---|---|---|
| Departure | Destination | **Change [%]** | | | |
| | | Contrails | Time | Fuel | Climate impact |
| EDDM | LBSF | -2.67 | 0.07 | 0.07 | -0.53 |
| EGLL | LTFM | NaN | NaN | NaN | NaN |
| EHAM | LIRF | NaN | NaN | NaN | NaN |
| EKCH | LPPT | NaN | NaN | NaN | NaN |
| ENGM | EBBR | NaN | NaN | NaN | NaN |
| ESGG | LOWS | -31,36 | 0.71 | 2.94 | -28.88 |
| EYVI | LSZH | -73.64 | 0.42 | 0.90 | -64.30 |
| LEMD | EIDW | NaN | NaN | NaN | NaN |
| LFPG | EVRA | -52.67 | 27.17 | 27.30 | -46.68 |
| LGAV | EFHK | 0 | 0 | 0 | 0 |
| LHBP | EETN | 0 | 0 | 0 | 0 |
| LROP | LMML | 0 | 0 | 0 | 0 |

**Table 4.4:** The percentage difference between flights that include avoidance areas and those that don't. A positive value represents an increase when avoidance areas are taken into account. These are the outcomes obtained for a winter night with a departure time of 02:00 - 01/01/2022. The avoidance areas range from $34,000$ ft to $42,000$ ft and the aircraft is forced to cruise at a minimum of $34,000$ ft. If no solution was obtained by the optimizer with the avoidance areas included, the values are NaN. The avoidance areas can be seen in A.2.

Table 4.4 presents two additional completed flight plans. It is worth noting that all deviations from the initial fuel-efficient route in this case led to a reduction in contrail formation and climate impact. However, note that in this case the EDDM-LBSF route only reduced the contrail formation by 2.67% compared to 84.92% during the day. This showcase that the same strategy, even for the same day can result in rather different results and that the outcomes are highly dependant on the atmospheric conditions. Additionally, there were no deviations from the initial flight plan for the LGAV-EFHK, LHBP-EETN, and LROP-LMML routes, which created 0, 49.15, and 71.09 km of contrails, respectively. This is likely due to the same reasons mentioned earlier.

#### 4.2.2.2 Flight Optimization - Spring

Next, Tables 4.5 and 4.6 show the results for a spring day (01/04/2022) during day and night time, respectively. The aircraft are forced to cruise above 34, 000 ft. The avoidance areas are illustrated in Figures A.3 and A.4.

| **Spring Day time - Forcing higher altitudes** | | | | | |
|---|---|---|---|---|---|
| Departure | Destination | **Change** [%] | | | |
| | | Contrails | Time | Fuel | Climate impact |
| EDDM | LBSF | 115.50 | 0.47 | 1.73 | 71.29 |
| EGLL | LTFM | -100 | -0.03 | 0.03 | -9.53 |
| EHAM | LIRF | -57.29 | 2.27 | 1.56 | -20.01 |
| EKCH | LPPT | -33.39 | 1.34 | 1.36 | -5.98 |
| ENGM | EBBR | -3.83 | 0.0 | 0.0 | -1.85 |
| ESGG | LOWS | -20.27 | 14.81 | 13.57 | -0.54 |
| EYVI | LSZH | NaN | NaN | NaN | NaN |
| LEMD | EIDW | 0 | 0 | 0 | 0 |
| LFPG | EVRA | NaN | NaN | NaN | NaN |
| LGAV | EFHK | -100 | 9.91 | 10.71 | -63.57 |
| LHBP | EETN | -81.11 | 24.65 | 24.68 | -59.81 |
| LROP | LMML | 161.70 | 0.12 | 0.62 | 34.60 |

**Table 4.5:** The percentage difference between flights that include avoidance areas and those that don't. A positive value represents an increase when avoidance areas are taken into account. These are the outcomes obtained for a spring day with a departure time of 13:00 - 01/04/2022. The avoidance areas range from 34, 000 ft to 42, 000 ft and the aircraft is forced to cruise at a minimum of 34, 000 ft. If no solution was obtained by the optimizer with the avoidance areas included, the values are NaN. The avoidance areas can be seen in A.3.

In all but two cases, optimized and feasible flight plans were generated, as shown in Table 4.5. Through a visual comparison between the avoidance areas for the spring and winter day in Figure A.3 and A.1, respectively, the coverage appears to be on a similar level. Hence, seemingly large avoidance areas that are projected onto the Earth do not necessarily result in a limited number of feasible and optimized flight plans.

Furthermore, in most cases where deviations from the initial flight plan occurred, there was a reduction in contrail creation and climate impact. Notably, the EGLL-LTFM and LGAV-EFHK routes completely eliminated contrail creation. However, the EGLL-LTFM route only reduced the climate impact by 9.53%, as the initial route only created 55.16 km of persistent contrails. Additionally, the LEMD-EIDW flight plan with avoidance areas did not deviate from the initial flight plan but still created 54.55 km of persistent contrails. For this atmospheric data, the EDDM-LBSF and LROP-LMML routes significantly increased contrail creation. As mentioned in 3.5, determining when the aircraft must begin cruising appears to be somewhat ambiguous. Therefore, if there are prolonged segments when the plane

is transitioning to/from cruising altitudes during takeoff and landing, it may fly in airspace that fulfills persistent contrail conditions for a large portion of the flight, where there are no avoidance areas. As a result, such cases can significantly increase total contrail creation if contrail conditions where fulfilled more frequently at lower altitudes compared to fuel-efficient altitudes.

| **Spring Night time - Forcing higher altitudes** | | | | | |
|---|---|---|---|---|---|
| Departure | Destination | **Change [%]** | | | |
| | | Contrails | Time | Fuel | Climate impact |
| EDDM | LBSF | 253.76 | 0.63 | 2.43 | 205.79 |
| EGLL | LTFM | NaN | NaN | NaN | NaN |
| EHAM | LIRF | 0 | 0 | 0 | 0 |
| EKCH | LPPT | -15.62 | 2.29 | 2.32 | -6.69 |
| ENGM | EBBR | 0 | 0 | 0 | 0 |
| ESGG | LOWS | 113.49 | 13.81 | 15.76 | 102.21 |
| EYVI | LSZH | NaN | NaN | NaN | NaN |
| LEMD | EIDW | 0 | 0 | 0 | 0 |
| LFPG | EVRA | -73.52 | 4.80 | 5.22 | -64.85 |
| LGAV | EFHK | -100 | 12.99 | 13.80 | -90.64 |
| LHBP | EETN | NaN | NaN | NaN | NaN |
| LROP | LMML | -2.11 | 0.08 | 0.08 | -1.16 |

**Table 4.6:** The percentage difference between flights that include avoidance areas and those that don't. A positive value represents an increase when avoidance areas are taken into account. These are the outcomes obtained for a spring night with a departure time of 02:00 - 01/04/2022. The avoidance areas range from 34,000 ft to 42,000 ft and the aircraft is forced to cruise at a minimum of 34,000 ft. If no solution was obtained by the optimizer with the avoidance areas included, the values are NaN. The avoidance areas can be seen in A.4.

The results presented in Table 4.6 demonstrate similar findings to previous cases. The EHAM-LIRF, ENGM-EBBR, and LEMD-EIDW routes showed no deviations from the initial flight plan and resulted in contrail creations of 83.73 km, 52.91 km, and 0 km, respectively. However, the initial flight plan for the LGAV-EFHK route resulted in 1488 km of persistent contrails, which were completely eliminated when the avoidance areas were included. This led to a significant reduction of 90.64% in climate impact. The rerouting of the LGAV-EFHK route can be visualized in Figure 4.5.

**Figure 4.5:** One example highlighted from the results with avoidance areas included combined with forcing the aircraft to cruise above 34,000 ft. The flight plan for the route LGAV-EFHK that includes avoidance areas results in a rerouting that flies the most west.

The visualization presented in Figure 4.5 illustrates that this method can lead to significant adjustments in both the latitudinal and longitudinal planes. The vertical profiles can be seen in A.3.2. Consequently, the optimization may require adjustments in not only altitude but also significant latitude and longitude changes. In this particular case, these adjustments resulted in a 13.80% increase in fuel consumption. However, it is important to note that in this case, these deviations resulted in a 90.64% decrease in climate impact.

#### 4.2.2.3 Flight Optimization - Summer

The results for a summer day (01/07/2022) during both day and night time are presented in Tables 4.7 and 4.8 respectively. The aircraft are forced to cruise at altitudes above 34,000 ft and the corresponding avoidance areas can be visualized in Figures A.5 and A.6.

| Summer Day time - Forcing higher altitudes | | | | | |
|---|---|---|---|---|---|
| Departure | Destination | Change [%] | | | |
| | | Contrails | Time | Fuel | Climate impact |
| EDDM | LBSF | 28.50 | 0.47 | 1.73 | 17.18 |
| EGLL | LTFM | NaN | NaN | NaN | NaN |
| EHAM | LIRF | 0 | 0 | 0 | 0 |
| EKCH | LPPT | -59.90 | 15.08 | 15.56 | -23.78 |
| ENGM | EBBR | NaN | NaN | NaN | NaN |
| ESGG | LOWS | NaN | NaN | NaN | NaN |
| EYVI | LSZH | NaN | NaN | NaN | NaN |
| LEMD | EIDW | NaN | NaN | NaN | NaN |
| LFPG | EVRA | NaN | NaN | NaN | NaN |
| LGAV | EFHK | NaN | NaN | NaN | NaN |
| LHBP | EETN | NaN | NaN | NaN | NaN |
| LROP | LMML | 0 | 0 | 0 | 0 |

**Table 4.7:** The percentage difference between flights that include avoidance areas and those that don't. A positive value represents an increase when avoidance areas are taken into account. These are the outcomes obtained for a summer day with a departure time of 13:00 - 01/07/2022. The avoidance areas range from 34,000 ft to 42,000 ft and the aircraft is forced to cruise at a minimum of 34,000 ft. If no solution was obtained by the optimizer with the avoidance areas included, the values are NaN. The avoidance areas can be seen in A.5.

Table 4.7 shows that only four outcomes from the optimizer resulted in optimized and feasible flight plans when the avoidance areas were included. Interestingly, when comparing the avoidance areas for all the cases, it can be observed that the examined summer data had the lowest coverage over Europe's airspace. This further emphasizes that the projected coverage of avoidance areas on Earth does not necessarily correspond to the number of feasible and optimized outcomes from the optimizer.

In this case, there were no deviations from the initial flight plans for the EHAM-LIRF and LROP-LMML routes, as these flights did not create any persistent contrails. Additionally, for this specific data, only one route experienced an improvement in contrail reduction. This highlights the variability of this strategy and its strong dependence on atmospheric conditions.

| Summer night time - Forcing higher altitudes | | | | | |
|---|---|---|---|---|---|
| Departure | Destination | Change [%] | | | |
| | | Contrail | Time | Fuel | Climate impact |
| EDDM | LBSF | 350.9 | 0.21 | 0.64 | 129.47 |
| EGLL | LTFM | -100 | -0.05 | 0.19 | -54.14 |
| EHAM | LIRF | 119.11 | 3.99 | 4.23 | 59.85 |
| EKCH | LPPT | NaN | NaN | NaN | NaN |
| ENGM | EBBR | 6.84 | 0.11 | 0.22 | 3.65 |
| ESGG | LOWS | 42.6 | 4.65 | 4.6 | 33.16 |
| EYVI | LSZH | NaN | NaN | NaN | NaN |
| LEMD | EIDW | 0 | 0 | 0 | 0 |
| LFPG | EVRA | -45.68 | 6.52 | 8.07 | -38.05 |
| LGAV | EFHK | NaN | NaN | NaN | NaN |
| LHBP | EETN | NaN | NaN | NaN | NaN |
| LROP | LMML | 0 | 0 | 0 | 0 |

**Table 4.8:** The percentage difference between flights that include avoidance areas and those that don't. A positive value represents an increase when avoidance areas are taken into account. These are the outcomes obtained for a summer night with a departure time of 13:00 - 01/07/2022. The avoidance areas range from 34,000 ft to 42,000 ft and the aircraft is forced to cruise at a minimum of 34,000 ft. If no solution was obtained by the optimizer with the avoidance areas included, the values are NaN. The avoidance areas can be seen in A.6.

Notice in Table 4.8 that this strategy yields more optimized outcomes compared to the results in Table 4.1. However, it is worth noting that this strategy led to significantly worse results for the EDDM-LBSF and ESGG-LOWS routes, as the resulting flight plans produced more contrails than the fuel-efficient plans. In contrast, when the entire airspace was considered using the other strategy, these routes resulted in a reduction in contrail creation. Nonetheless, this approach did identify a potentially improved flight plan for the LFPG-EVRA route, whereas the other strategy failed to produce any results. Consequently, while this approach may produce more results, they may not necessarily be better than those obtained by considering the entire airspace.

#### 4.2.2.4 Flight Optimization - Fall

Finally, the results for a fall day (01/10/2022) during both day and night time are presented in Tables 4.9 and 4.10 respectively. The aircraft are forced to cruise at altitudes above 34,000 ft and the corresponding avoidance areas can be visualized in Figures 4.1 and A.7.

| Fall Day time - Forcing higher altitudes | | | | | |
|---|---|---|---|---|---|
| Departure | Destination | Change [%] | | | |
| | | Contrails | Time | Fuel | Climate impact |
| EDDM | LBSF | 78.24 | 0.47 | 1.73 | 51.59 |
| EGLL | LTFM | NaN | NaN | NaN | NaN |
| EHAM | LIRF | 79.24 | 0.15 | 0.55 | 8.90 |
| EKCH | LPPT | 0 | 0 | 0 | 0 |
| ENGM | EBBR | 0 | 0 | 0 | 0 |
| ESGG | LOWS | 0 | 0 | 0 | 0 |
| EYVI | LSZH | -74.18 | 13.11 | 13.25 | -38.06 |
| LEMD | EIDW | 0 | 0 | 0 | 0 |
| LFPG | EVRA | -48.27 | 6.82 | 6.47 | -0.32 |
| LGAV | EFHK | NaN | NaN | NaN | NaN |
| LHBP | EETN | -18.48 | 2.41 | 2.33 | -1.46 |
| LROP | LMML | NaN | NaN | NaN | NaN |

**Table 4.9:** The percentage difference between flights that include avoidance areas and those that don't. A positive value represents an increase when avoidance areas are taken into account. These are the outcomes obtained for a fall day with a departure time of 13:00 - 01/10/2022. The avoidance areas range from 34,000 ft to 42,000 ft and the aircraft is forced to cruise at a minimum of 34,000 ft. If no solution was obtained by the optimizer with the avoidance areas included, the values are NaN. The avoidance areas can be seen in 4.1.

Table 4.9 presents results that are similar to the previous cases discussed, where three of the flight plans showed a reduction in contrail creation. However, it should be noted that for the LFPG-EVRA flight plan, although there was a reduction in contrail creation by 48.27%, the reduction in climate impact was negligible. This is because the initial flight only created 49.55 km of persistent contrails, with an increase of 6.47% in fuel consumption. Additionally, keep in mind that the impact of persistent contrails is lower during the daytime, and thus, this reduction in contrail creation will not lead to as significant reduction in climate impact.

| Fall night time - Forcing higher altitudes | | | | | |
|---|---|---|---|---|---|
| Departure | Destination | Change [%] | | | |
| | | Contrail | Time | Fuel | Climate impact |
| EDDM | LBSF | 140.06 | 0.64 | 2.30 | 112.32 |
| EGLL | LTFM | NaN | NaN | NaN | NaN |
| EHAM | LIRF | -73.72 | 22.11 | 21.65 | -64.65 |
| EKCH | LPPT | NaN | NaN | NaN | NaN |
| ENGM | EBBR | NaN | NaN | NaN | NaN |
| ESGG | LOWS | NaN | NaN | NaN | NaN |
| EYVI | LSZH | -11.42 | 0.04 | 0.09 | -8.07 |
| LEMD | EIDW | NaN | NaN | NaN | NaN |
| LFPG | EVRA | -51.21 | 6.67 | 6.82 | -43.50 |
| LGAV | EFHK | -48.55 | 17.03 | 17.93 | -37.61 |
| LHBP | EETN | 48.77 | 0.09 | 0.22 | 28.98 |
| LROP | LMML | -89.38 | 14.02 | 14.04 | -82.55 |

**Table 4.10:** The percentage difference between flights that include avoidance areas and those that don't. A positive value represents an increase when avoidance areas are taken into account. These are the outcomes obtained for a fall night with a departure time of 02:00 - 01/10/2022. The avoidance areas range from 34,000 ft to 42,000 ft and the aircraft is forced to cruise at a minimum of 34,000 ft. If no solution was obtained by the optimizer with the avoidance areas included, the values are NaN. The avoidance areas can be seen in A.7.

The results in Table 4.10 showcase that this strategy can yield more optimized outcomes than considering the entire airspace, as shown in Table 4.2. However, for all outcomes that both strategies found, considering the whole airspace resulted in a higher contrail reduction. Nevertheless, this strategy found feasible flight plans with reduced contrail creation that the other strategy failed to find. One of these examples is the route between LROP to LMML that exhibits a significant reduction in total climate impact. The initial fuel-efficient flight plan created approximately 1050 km of persistent contrails, which is equivalent to roughly 75% of the total air distance. This is due to the fact that the initial route passes through a large cluster, as depicted in Figure 4.6.

**Figure 4.6:** One example highlighted from the results with avoidance areas included combined with forcing the aircraft to cruise above 34, 000 ft. The flight plan that includes avoidance areas results in a rerouting that flies the most south for the LROP-LMML route.

As can be seen in Figure 4.6, the rerouted flight exhibits deviations in both the latitudinal and longitudinal planes, in addition to altitude corrections. The vertical profiles can be seen in A.3.3. This illustrates, once again, that optimization may require adjustments in not only altitude but also latitude and longitude.

# 5
# Conclusion

To begin with, the strategies presented in this thesis can be utilized to find alternative flight plans that reduce the persistent contrail creation and climate impact. For some of the notable cases examined, the climate impact was reduced by over 80%, with increased fuel consumption of around 14%. Moreover, there were instances where contrail formation could be significantly or completely reduced with negligible increments in flight duration or fuel consumption.

However, the strategies presented have different advantages, depending on the atmospheric conditions. For the cases presented in the results, by considering the whole airspace, all plans deviating from their original fuel-efficient trajectory resulted in a reduction in contrail creation. On the other hand, the strategy may yield a limited number of optimized and feasible outcomes. There are two likely explanations for missing outcomes. The first one, the avoidance areas may interfere with flight regulation, rendering the flight plan infeasible. Secondly, the high complexity introduced by the avoidance areas may prevent the optimizer from finding an optimal feasible solution within the allowed computational time. The other strategy presented, by creating avoidance areas above $34,000$ ft and then forcing the aircraft to cruise above this altitude, may yield more outcomes. However, these outcomes may result in a lower reduction in contrail creation compared to the other strategy.

Moreover, there are several options to adjust the strategies presented. For example, a different temporal threshold, the range of avoidance areas, and forcing the aircraft to cruise at different altitudes. Since the avoidance areas often cover a significant portion of the airspace, the strategies proposed in this thesis may not always lead to a reduction in persistent contrail formation under certain atmospheric conditions. To overcome this, one approach is to generate multiple flight plan suggestions in parallel with different strategies, and then select the preferred option that achieves a reasonable balance between reduced contrail formation and increased flight time and fuel consumption. As demonstrated in 4.2.2, there were cases where the contrail formation was drastically reduced with a relatively small increase in flight time and fuel consumption. However, there were also instances where the contrail formation increased. In such cases, the original flight plan should be used instead.

Furthermore, since the avoidance areas are set as constraints in the optimizer, rather than using a penalty function, it is possible for some global optimal solutions to be missed. For instance, imagine that the contrail conditions are fulfilled at 26,000 ft all around the earth or a very large area. In that case, the optimizer will never

return a flight path that crosses this area, even if the airspace above it is entirely contrail-free. Or if the aircraft is forced to cruise above 34, 000 ft, the plan will be infeasible since it will have to cross the avoidance areas. Consequently, there may be flight trajectories that pass through these avoidance areas, which have a lower climate impact than those constrained to fly below 26,000 feet, that the optimizer misses. Furthermore, implementing the areas as a penalty function would remove the possibility of rendering the flight infeasible, if they interfere with other flight regulations. Consequently, the whole airspace can be considered without the risk of rendering a flight plan infeasible. Therefore, in the future, methods to incorporate these avoidance areas as penalty areas instead could result in more balanced results with regard to time, fuel cost, and contrail creation.

## 5.1 Future work

First of all, implementing strategies to avoid contrails could reduce aviation's impact on the climate. This thesis assumed a high precision of persistent contrail conditions based on reanalysis of weather data, specifically ERA5 from ECMWF. However, recent research [36] indicates that the number and duration of persistent contrail condition regions derived from reanalysis data could be overestimated. This overestimation is likely present in forecasts using numerical weather prediction (NWP) as well [37]. As a result, effective real-world implementation of contrail avoidance strategies necessitates an accurate forecast of persistent contrail condition regions, which may require real-time observations or satellite image detection. However, regulations that all commercial aircraft must carry equipment capable of measuring ambient humidity and temperature could complement or enhance weather forecasts.

Furthermore, more research is needed to account for the uncertainties surrounding the contrail impact when making decisions about contrail avoidance. Furthermore, it is worth exploring a more comprehensive climate-focused trajectory optimization that considers the impact of other substances like $NO_x$, in addition to contrails and $CO_2$.

The proposed strategies in this thesis may not be applicable to longer flights. For instance, consider a 12-hour flight, then the airspace that satisfies the contrail conditions may significantly change during the flight. Creating avoidance areas by analyzing a 12-hour time frame would be inaccurate since the conditions might have changed drastically by the time the aircraft enters a particular area. Instead, custom avoidance areas can be created for specific flights by identifying the likely locations of the aircraft at different time points during the flight. This approach enables the creation of tailored avoidance areas for specific areas and time points where the aircraft is expected to be present.

Finally, as mentioned earlier, there are potential benefits to implementing the avoidance areas as a penalty function instead of constraints. Therefore, in the future, methods to incorporate these avoidance areas as penalty areas instead could result in better outcomes for flight time, fuel cost, and contrail creation. Keep in mind that

Jeppesen's optimizer used in this thesis is industry-leading and such modifications could be feasible implementations in the future.

# Bibliography


[1] S. Ornes, "How to curb the climate heating by contrails," *Science News Explores*, Apr. 27, 2020. [Online]. Available: https://www.snexplores.org/article/how-to-curb-the-climate-heating-by-contrails.

[2] D. Lee *et al.*, "The contribution of global aviation to anthropogenic climate forcing for 2000 to 2018," *Atmospheric Environment*, vol. 244, p. 117 834, 2021. DOI: 10.1016/j.atmosenv.2020.117834.

[3] K. Caldeira and I. McKay, "Contrails: Tweaking flight altitude could be a climate win," *Nature*, vol. 593, no. 7859, p. 341, May 2021, ISSN: 1476-4687 (online). DOI: https://doi.org/10.1038/d41586-021-01339-7. [Online]. Available: https://www.nature.com/articles/d41586-021-01339-7.

[4] E. Schmidt, *Die entstehung von eisnebel aus den auspuffgasen von flugmotoren*, Eintrag von Ulrich Schumann, zur Sicherstellung des Zugangs zu diesem wissenschaftshistorisch wichtigen Dokument; mit Zustimmung des Rechteinhabers (Nachfolger des Oldenbourg Verlags), 1941. [Online]. Available: https://elib.dlr.de/107948/.

[5] H. Appleman, "The formation of exhaust condensation trails by jet aircraft," *Bulletin of the American Meteorological Society*, vol. 34, no. 1, pp. 14–20, 1953. DOI: https://doi.org/10.1175/1520-0477-34.1.14. [Online]. Available: https://journals.ametsoc.org/view/journals/bams/34/1/1520-0477-34_1_14.xml.

[6] K. Gierens, "Theory of contrail formation for fuel cells," *Aerospace*, vol. 8, no. 6, 2021, ISSN: 2226-4310. DOI: 10.3390/aerospace8060164. [Online]. Available: https://www.mdpi.com/2226-4310/8/6/164.

[7] R. Teoh, M. E. Stettler, A. Majumdar, U. Schumann, B. Graves, and A. M. Boies, "A methodology to relate black carbon particle number and mass emissions," *Journal of Aerosol Science*, vol. 132, pp. 44–59, 2019, ISSN: 0021-8502. DOI: https://doi.org/10.1016/j.jaerosci.2019.03.006. [Online]. Available: https://www.sciencedirect.com/science/article/pii/S0021850218304336.

[8] N. Y. Chen, B. Sridhar, and H. K. Ng, "Tradeoff between contrail reduction and emissions in united states national airspace," *Journal of Aircraft*, vol. 49, no. 5, pp. 1367–1375, 2012. DOI: 10.2514/1.C031680. eprint: https://doi.org/10.2514/1.C031680. [Online]. Available: https://doi.org/10.2514/1.C031680.

[9] M. Ponater, S. Marquart, and R. Sausen, "Contrails in a comprehensive global climate model: Parameterization and radiative forcing results," *Journal of Geophysical Research: Atmospheres*, vol. 107, no. D13, ACL 2-1-ACL 2–15,

2002. DOI: https://doi.org/10.1029/2001JD000429. eprint: https://agupubs.onlinelibrary.wiley.com/doi/pdf/10.1029/2001JD000429. [Online]. Available: https://agupubs.onlinelibrary.wiley.com/doi/abs/10.1029/2001JD000429.

[10] K. M. Gierens, U. Schumann, H. G. Smit, M. Helten, and G. Zängl, "Determination of humidity and temperature fluctuations based on mozaic data and parametrisation of persistent contrail coverage for general circulation models," *Annales Geophysicae*, vol. 15, no. 8, pp. 1057–1066, 1997. DOI: 10.1007/s00585-997-1057-3.

[11] O. A. Alduchov and R. E. Eskridge, "Improved magnus form approximation of saturation vapor pressure," *Journal of Applied Meteorology and Climatology*, vol. 35, no. 4, pp. 601–609, 1996. DOI: https://doi.org/10.1175/1520-0450(1996)035<0601:IMFAOS>2.0.CO;2. [Online]. Available: https://journals.ametsoc.org/view/journals/apme/35/4/1520-0450_1996_035_0601_imfaos_2_0_co_2.xml.

[12] [Online]. Available: https://www.climate.gov/maps-data/climate-data-primer/predicting-climate/climate-forcing.

[13] [Online]. Available: https://climate.mit.edu/explainers/radiative-forcing.

[14] [Online]. Available: https://www.epa.gov/ghgemissions/understanding-global-warming-potentials.

[15] M. Ponater, M. Bickel, L. Bock, and U. Burkhardt, "Towards determining the contrail cirrus efficacy," *Aerospace*, vol. 8, no. 2, p. 42, 2021. DOI: 10.3390/aerospace8020042.

[16] D. Lee *et al.*, "The contribution of global aviation to anthropogenic climate forcing for 2000 to 2018," *Atmospheric Environment*, vol. 244, p. 117 834, 2021, ISSN: 1352-2310. DOI: https://doi.org/10.1016/j.atmosenv.2020.117834. [Online]. Available: https://www.sciencedirect.com/science/article/pii/S1352231020305689.

[17] I. Sanz-Morère, S. D. Eastham, F. Allroggen, R. L. Speth, and S. R. H. Barrett, "Impacts of multi-layer overlap on contrail radiative forcing," *Atmospheric Chemistry and Physics*, vol. 21, no. 3, pp. 1649–1681, 2021. DOI: 10.5194/acp-21-1649-2021. [Online]. Available: https://acp.copernicus.org/articles/21/1649/2021/.

[18] K. Gierens and M. Vázquez-Navarro, "Statistical analysis of contrail lifetimes from a satellite perspective," *Meteorologische Zeitschrift*, vol. 27, Jan. 2017. DOI: 10.1127/metz/2018/0888.

[19] R. Teoh, U. Schumann, and M. E. J. Stettler, "Beyond contrail avoidance: Efficacy of flight altitude changes to minimise contrail climate forcing," *Aerospace*, vol. 7, no. 9, 2020, ISSN: 2226-4310. DOI: 10.3390/aerospace7090121. [Online]. Available: https://www.mdpi.com/2226-4310/7/9/121.

[20] M. H, B. A, and B. L, "Ground-based observations for the validation of contrails and cirrus detection in satellite imagery," *Atmospheric Measurement Techniques Discussions*, vol. 3, Dec. 2009. DOI: 10.5194/amt-3-655-2010.

[21] U. Schumann *et al.*, "Properties of individual contrails: A compilation of observations and some comparisons," *Atmospheric Chemistry and Physics*, vol. 17,

no. 1, pp. 403–438, 2017. DOI: 10.5194/acp-17-403-2017. [Online]. Available: https://acp.copernicus.org/articles/17/403/2017/.

[22] [Online]. Available: https://www.skybrary.aero/articles/altitude-flight-level-and-height.

[23] [Online]. Available: https://www.weather.gov/media/epz/wxcalc/pressureAltitude.pdf.

[24] [Online]. Available: https://www.faa.gov/regulations_policies/handbooks_manuals/aviation/phak.

[25] [Online]. Available: https://www.faa.gov/regulations_policies/handbooks_manuals/aviation/instrument_procedures_handbook.

[26] [Online]. Available: https://www.skybrary.aero/articles/sids-and-stars.

[27] D. Krasnoshchekov and V. Polishchuk, "Order-k -hulls and -shapes," *Information Processing Letters*, vol. 114, no. 1, pp. 76–83, 2014, ISSN: 0020-0190. DOI: https://doi.org/10.1016/j.ipl.2013.07.023. [Online]. Available: https://www.sciencedirect.com/science/article/pii/S0020019013002123.

[28] H. Edelsbrunner and E. Mücke, *Three-dimensional alpha shapes*, 1994. arXiv: math/9410208 [math.CO].

[29] [Online]. Available: https://graphics.stanford.edu/courses/cs268-11-spring/handouts/AlphaShapes/as_fisher.pdf.

[30] [Online]. Available: https://doc.cgal.org/latest/Alpha_shapes_2/index.html.

[31] [Online]. Available: https://cds.climate.copernicus.eu/cdsapp#!/dataset/reanalysis-era5-pressure-levels?tab=overview.

[32] Apr. 2023. [Online]. Available: https://docs.xarray.dev/en/stable/generated/xarray.DataArray.interp.html.

[33] [Online]. Available: https://docs.scipy.org/doc/scipy/reference/generated/scipy.interpolate.LinearNDInterpolator.html#scipy.interpolate.LinearNDInterpolator.

[34] R. Teoh *et al.*, "Aviation contrail climate effects in the north atlantic from 2016 to 2021," *Atmospheric Chemistry and Physics*, vol. 22, no. 16, pp. 10 919–10 935, 2022. DOI: 10.5194/acp-22-10919-2022. [Online]. Available: https://acp.copernicus.org/articles/22/10919/2022/.

[35] Environmental and E. S. I. (EESI), *Issue brief: The growth in greenhouse gas emissions from commercial aviation (2019, revised 2022)*. [Online]. Available: https://www.eesi.org/papers/view/fact-sheet-the-growth-in-greenhouse-gas-emissions-from-commercial-aviation.

[36] A. Agarwal, V. R. Meijer, S. D. Eastham, R. L. Speth, and S. R. Barrett, "Reanalysis-driven simulations may overestimate persistent contrail formation by 100%–250%," *Environmental Research Letters*, vol. 17, no. 1, p. 014 045, 2022. DOI: 10.1088/1748-9326/ac38d9.

[37] V. R. Meijer *et al.*, "Contrail coverage over the united states before and during the covid-19 pandemic," *Environmental Research Letters*, vol. 17, no. 3, p. 034 039, 2022. DOI: 10.1088/1748-9326/ac26f0.

# A

# Appendix

## A.1 Avoidance areas

### A.1.1 Avoidance areas - Winter

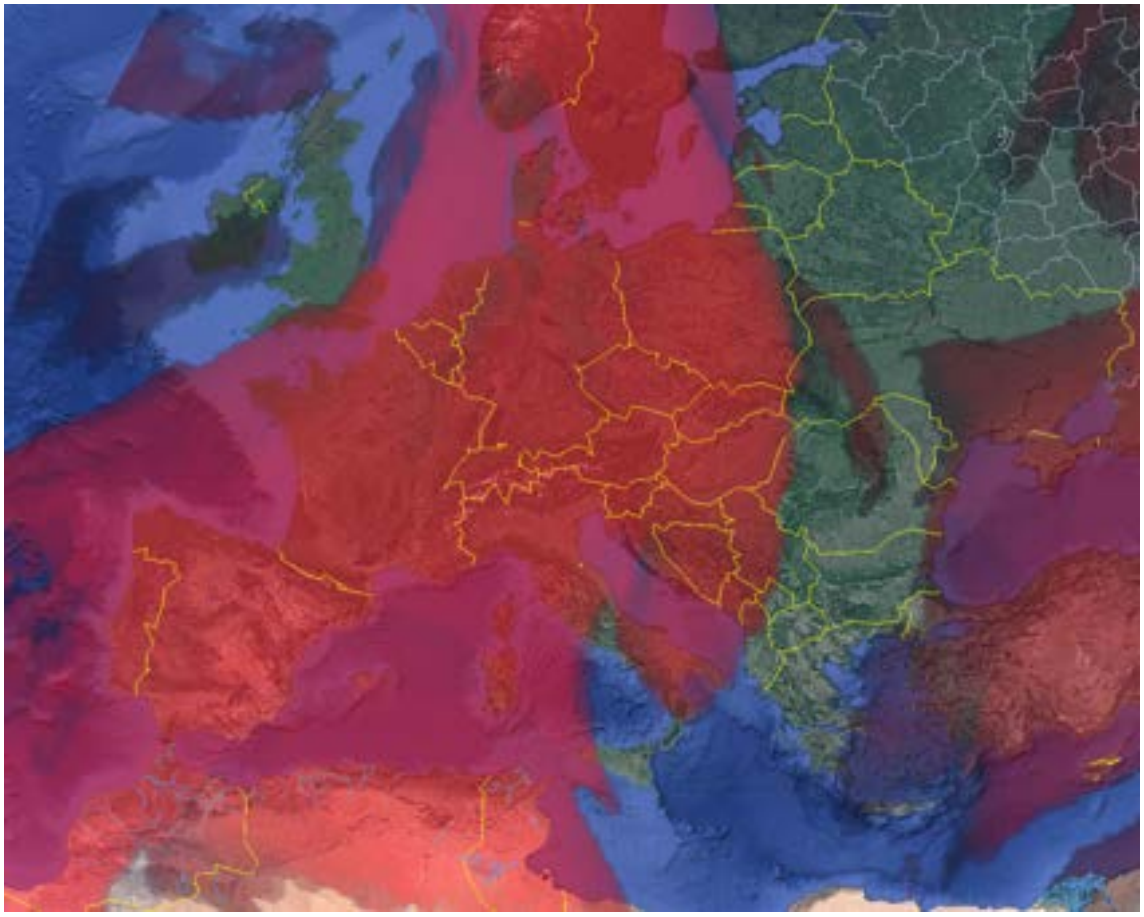

**Figure A.1:** Europe's airspace is marked with gradient shades of red to indicate the avoidance areas. These areas are formed through the clustering of a 2 out of 3 temporal threshold with $\alpha = 4.5$ in the alpha shape clustering method described in 3.3. The atmospheric conditions for the avoidance areas are applicable for the date range of 01/01/2022 between 13:00 - 15:00.

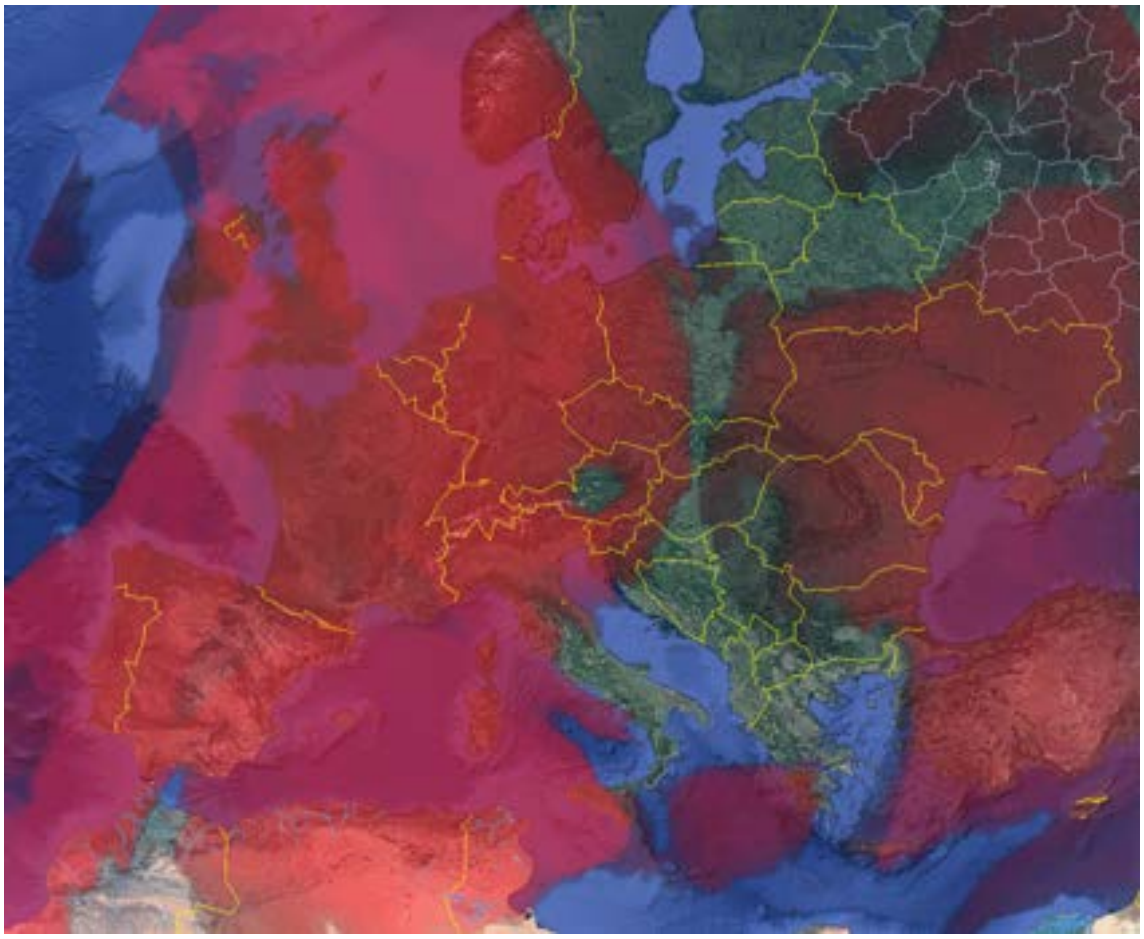

**Figure A.2:** Europe's airspace is marked with gradient shades of red to indicate the avoidance areas. These areas are formed through the clustering of a 2 out of 3 temporal threshold with $\alpha = 4.5$ in the alpha shape clustering method described in 3.3. The atmospheric conditions for the avoidance areas are applicable for the date range of 01/01/2022 between 02:00 - 04:00.

### A.1.2 Avoidance areas - Spring

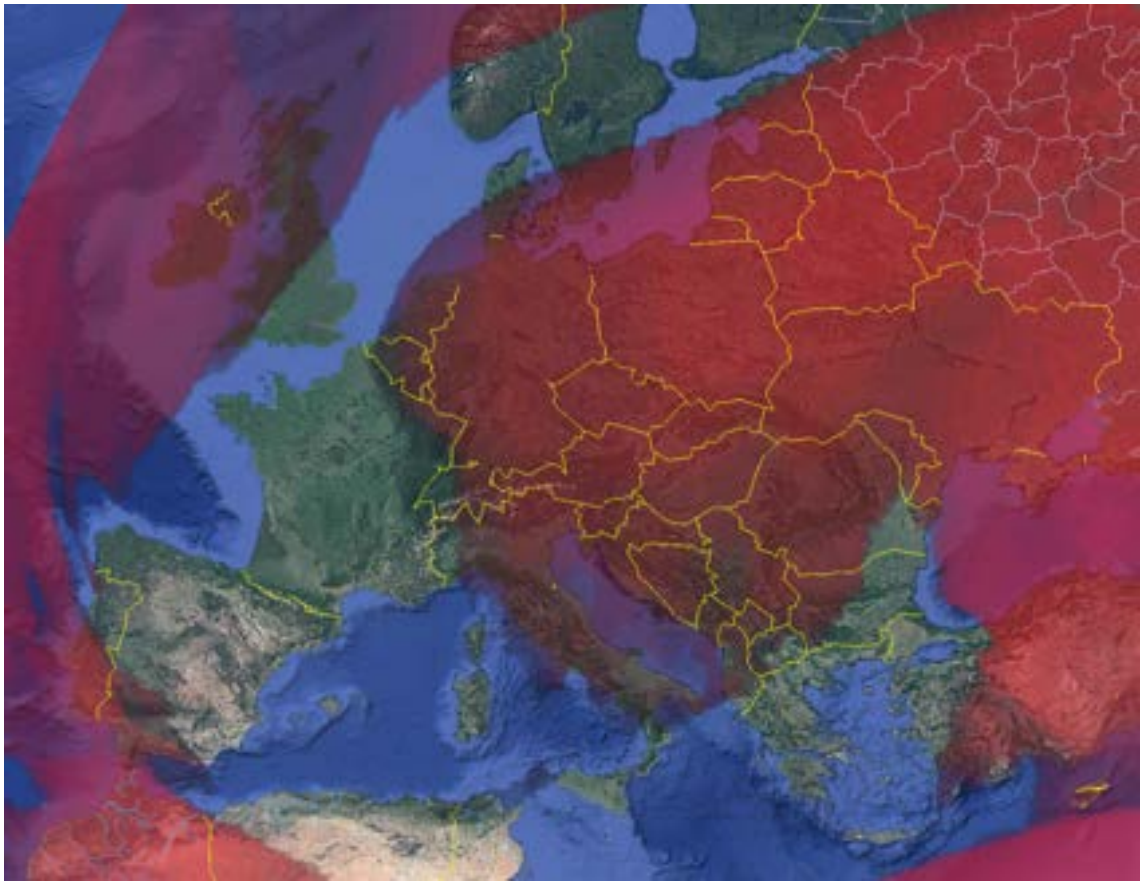

**Figure A.3:** Europe's airspace is marked with gradient shades of red to indicate the avoidance areas. These areas are formed through the clustering of a 2 out of 3 temporal threshold with $\alpha = 4.5$ in the alpha shape clustering method described in 3.3. The atmospheric conditions for the avoidance areas are applicable for the date range of 01/04/2022 between 13:00 - 15:00.

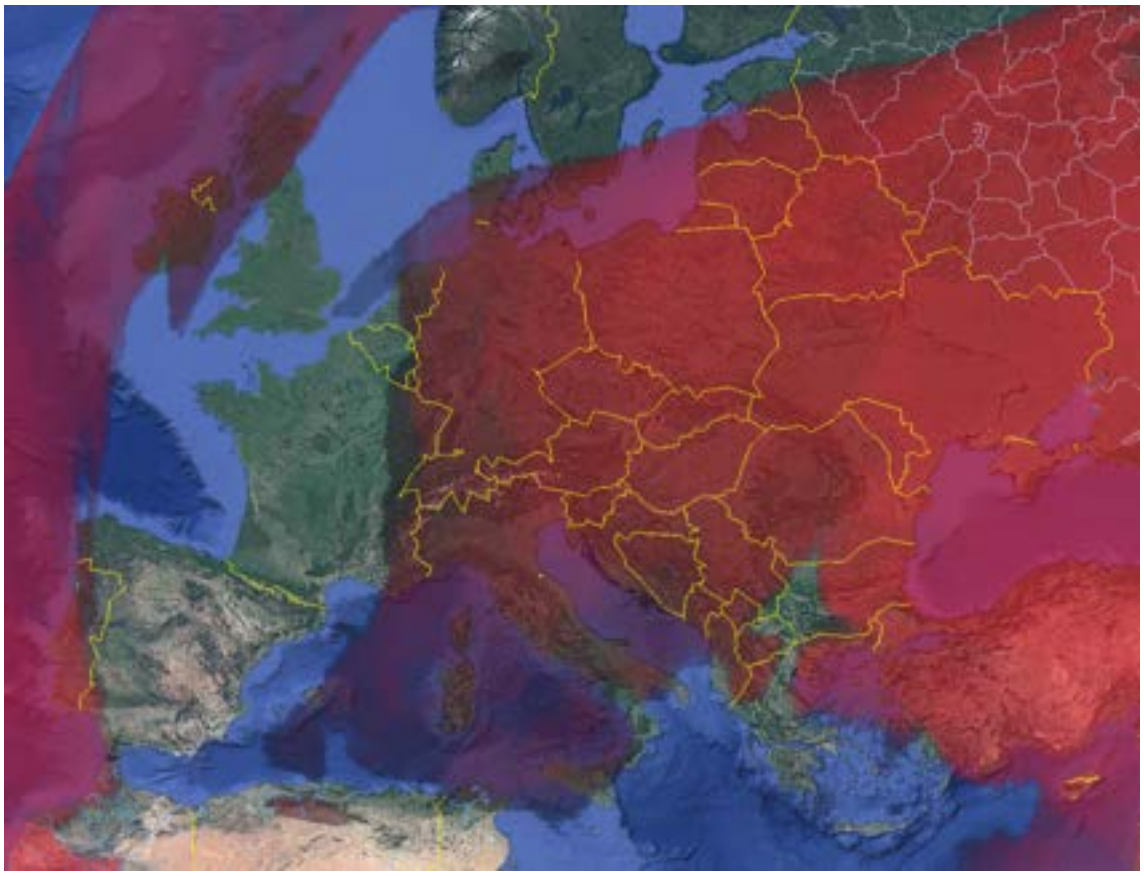

**Figure A.4:** Europe's airspace is marked with gradient shades of red to indicate the avoidance areas. These areas are formed through the clustering of a 2 out of 3 temporal threshold with $\alpha = 4.5$ in the alpha shape clustering method described in 3.3. The atmospheric conditions for the avoidance areas are applicable for the date range of 01/04/2022 between 02:00 - 04:00.

### A.1.3 Avoidance areas - Summer

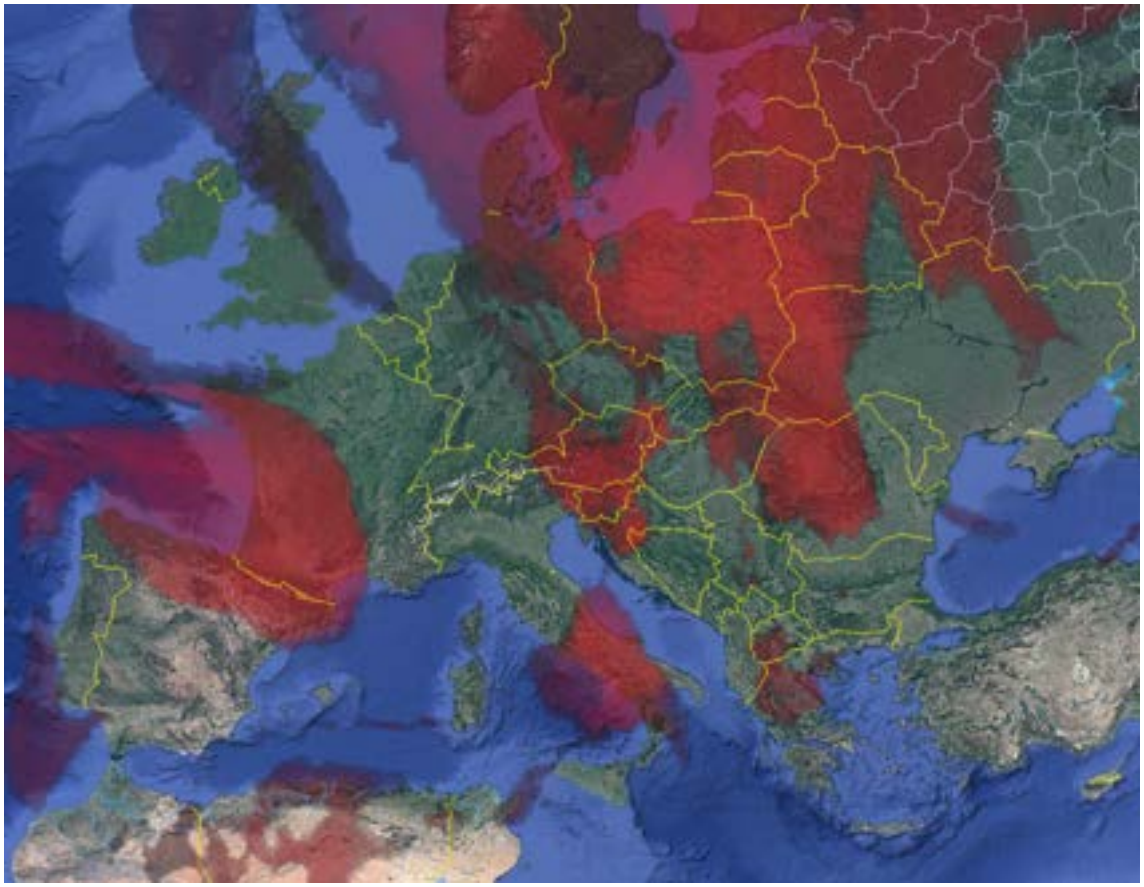

**Figure A.5:** Europe's airspace is marked with gradient shades of red to indicate the avoidance areas. These areas are formed through the clustering of a 2 out of 3 temporal threshold with $\alpha = 4.5$ in the alpha shape clustering method described in 3.3. The atmospheric conditions for the avoidance areas are applicable for the date range of 01/07/2022 between 13:00 - 15:00.

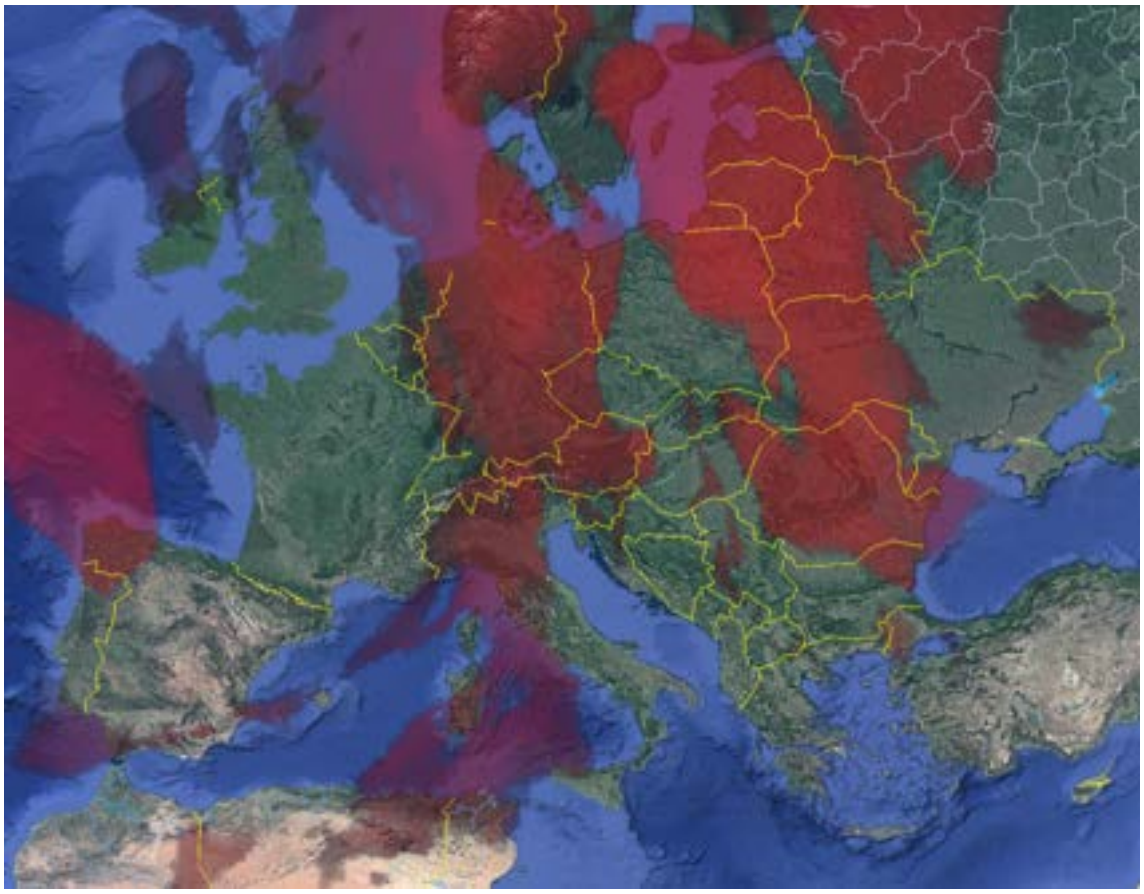

**Figure A.6:** Europe's airspace is marked with gradient shades of red to indicate the avoidance areas. These areas are formed through the clustering of a 2 out of 3 temporal threshold with $\alpha = 4.5$ in the alpha shape clustering method described in 3.3. The atmospheric conditions for the avoidance areas are applicable for the date range of 01/07/2022 between 02:00 - 04:00.

### A.1.4 Avoidance areas - Fall

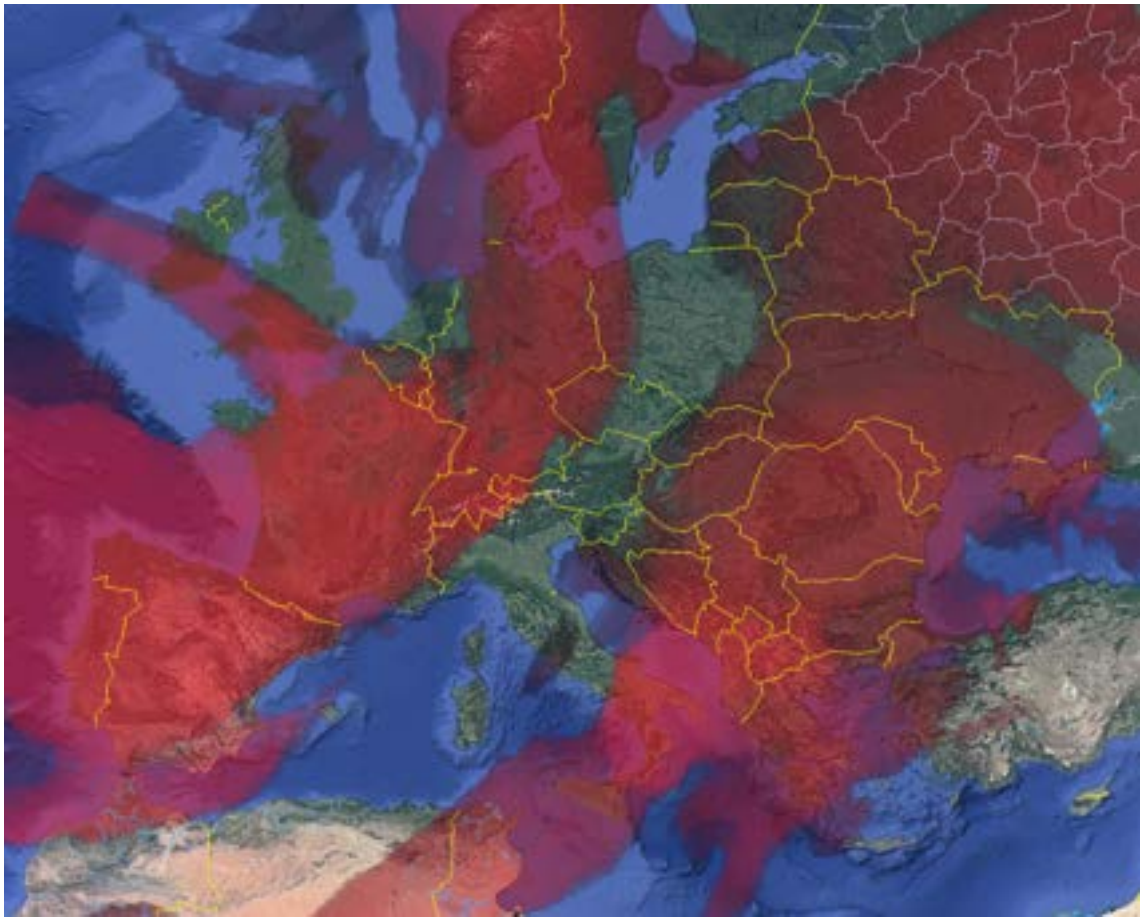

**Figure A.7:** Europe's airspace is marked with gradient shades of red to indicate the avoidance areas. These areas are formed through the clustering of a 2 out of 3 temporal threshold with $\alpha = 4.5$ in the alpha shape clustering method described in 3.3. The atmospheric conditions for the avoidance areas are applicable for the date range of 01/10/2022 between 02:00 - 04:00.

## A.2 Additional Results from Simulation

| **Summer Night time - Forcing altitude and different Temporal threshold** | | | | | |
|---|---|---|---|---|---|
| Departure | Destination | **Change [%]** | | | |
| | | Time | Fuel | Contrails | Climate impact |
| EDDM | LBSF | 406.45 | 0.28 | 0.76 | 149.95 |
| EGLL | LTFM | NaN | NaN | NaN | NaN |
| EHAM | LIRF | -39.69 | 6.09 | 6.08 | -16.08 |
| EKCH | LPPT | NaN | NaN | NaN | NaN |
| ENGM | EBBR | NaN | NaN | NaN | NaN |
| ESGG | LOWS | NaN | NaN | NaN | NaN |
| EYVI | LSZH | NaN | NaN | NaN | NaN |
| LEMD | EIDW | 0 | 0 | 0 | 0 |
| LFPG | EVRA | NaN | NaN | NaN | NaN |
| LGAV | EFHK | NaN | NaN | NaN | NaN |
| LHBP | EETN | NaN | NaN | NaN | NaN |
| LROP | LMML | 0 | 0 | 0 | 0 |

**Table A.1:** The percentage difference between flights that include avoidance areas and those that don't. A positive value represents an increase when avoidance areas are taken into account. These are the outcomes obtained for a summer night with a departure time of 02:00 - 01/07/2022. In this case, a temporal threshold of 1 out of 3 hours was applied. The avoidance areas can be seen in 4.2b.

## A.3 Vertical Profiles

### A.3.1 Summer night - Whole Airspace EGLL-LFTM

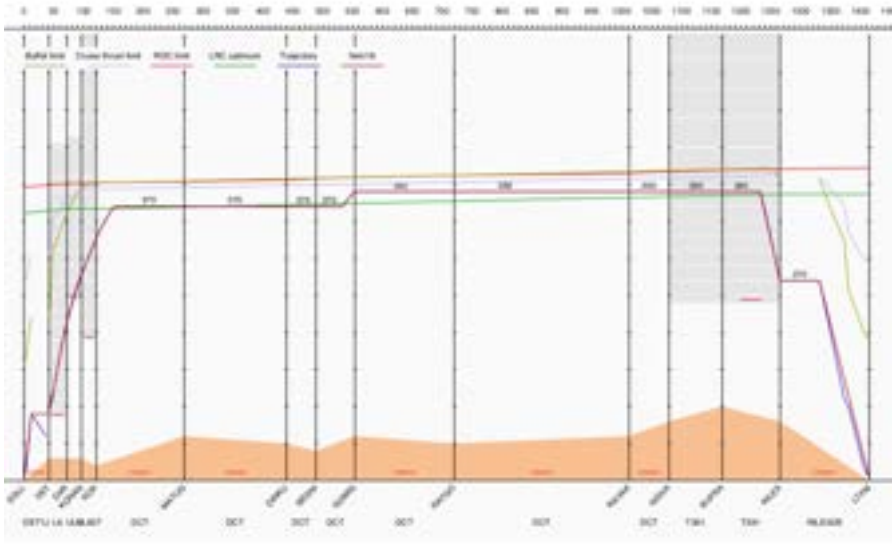

**Figure A.8:** The vertical profile for the EGLL-LFTM route during a summer night **without** avoidance areas. Note that the trajectory (dark blue) can be hidden by item18 (red).

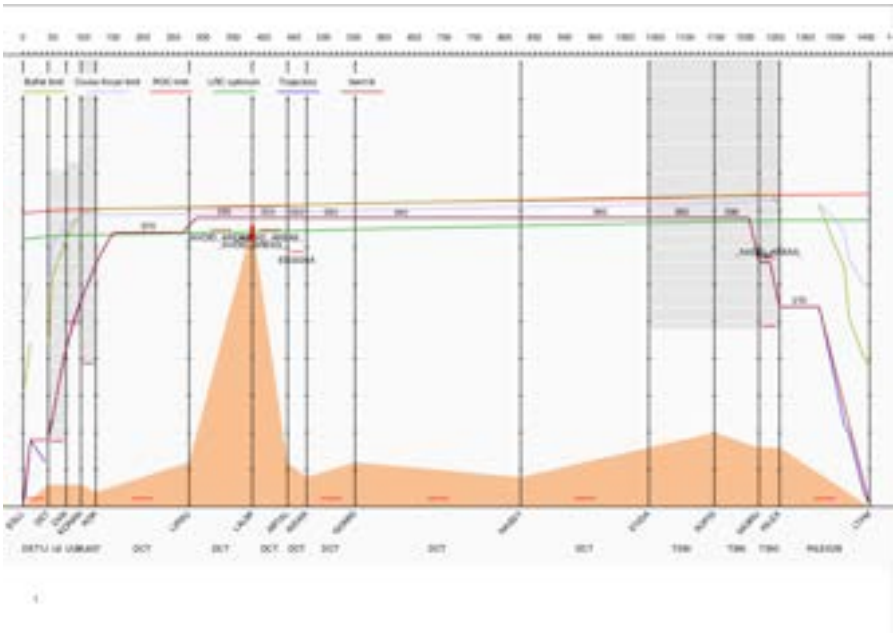

**Figure A.9:** The vertical profile for the EGLL-LFTM route during a summer night **with** avoidance areas. Note that the trajectory (dark blue) can be hidden by item18 (red).

### A.3.2 Spring night - Force Airspace LGAV-EFHK

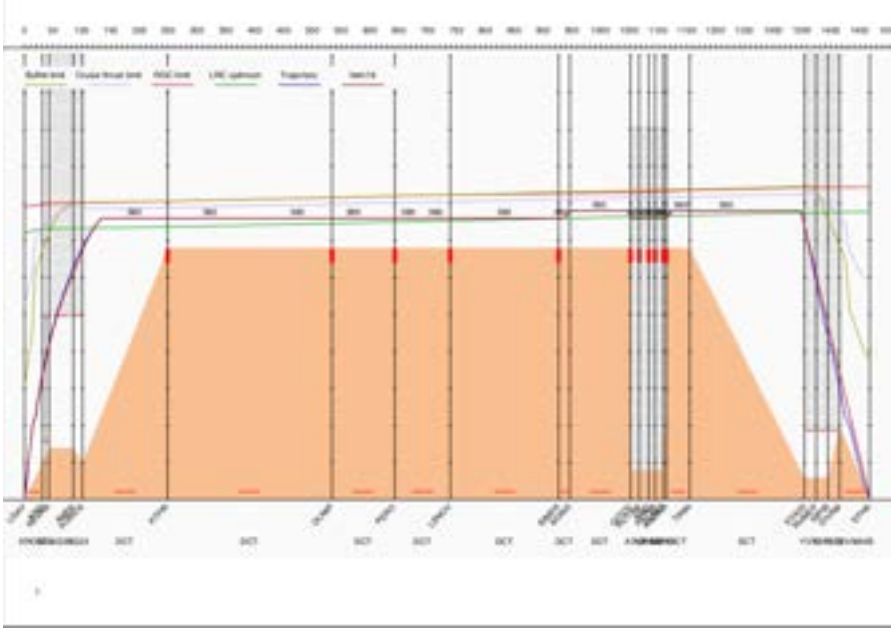

**Figure A.10:** The vertical profile for the LGAV-EFHK route during a spring night **without** avoidance areas. Note that the trajectory (dark blue) can be hidden by item18 (red).

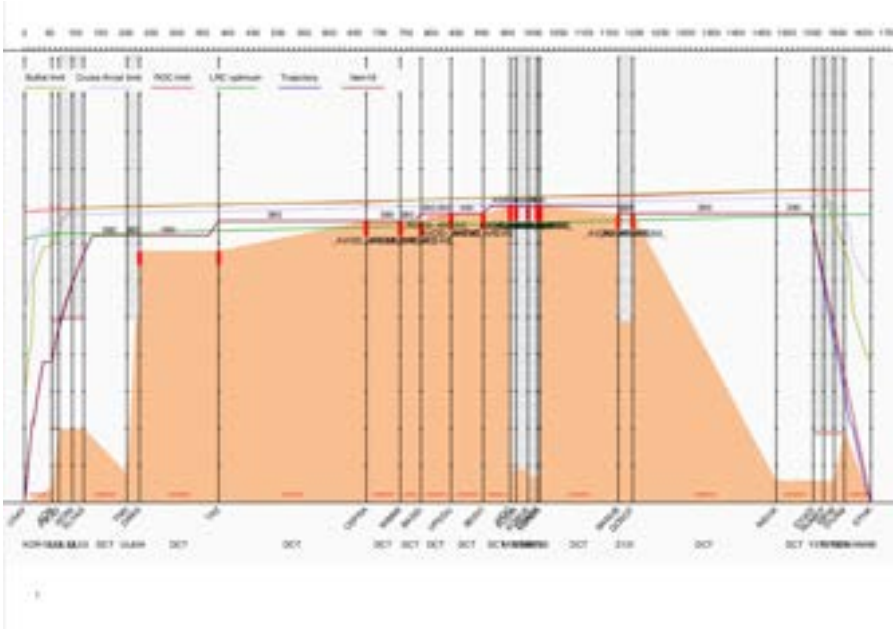

**Figure A.11:** The vertical profile for the LGAV-EFHK route during a spring night **with** avoidance areas. Note that the trajectory (dark blue) can be hidden by item18 (red).

### A.3.3 Fall night - Force Airspace LROP-LMML

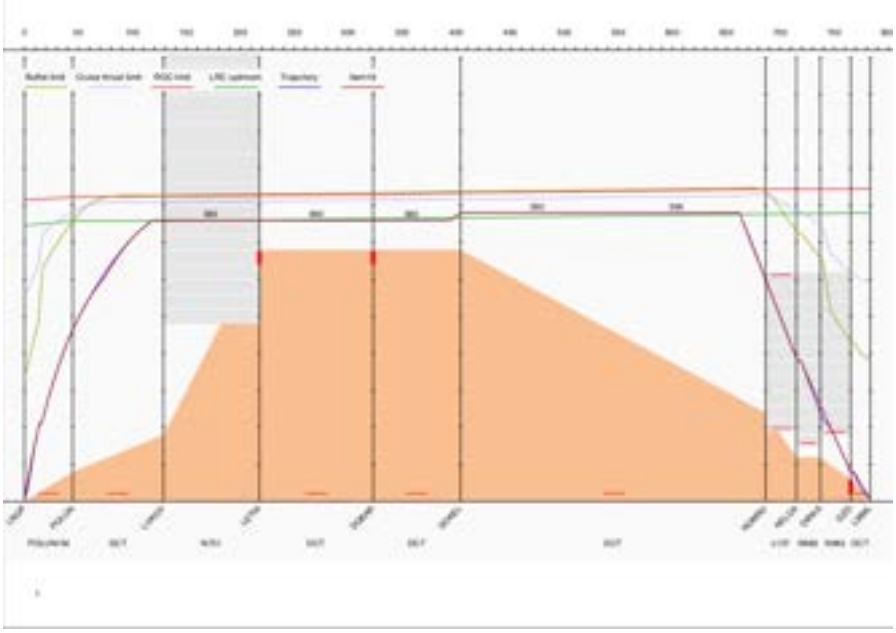

**Figure A.12:** The vertical profile for the LROP-LMML route during a fall night **without** avoidance areas. Note that the trajectory (dark blue) can be hidden by item18 (red).

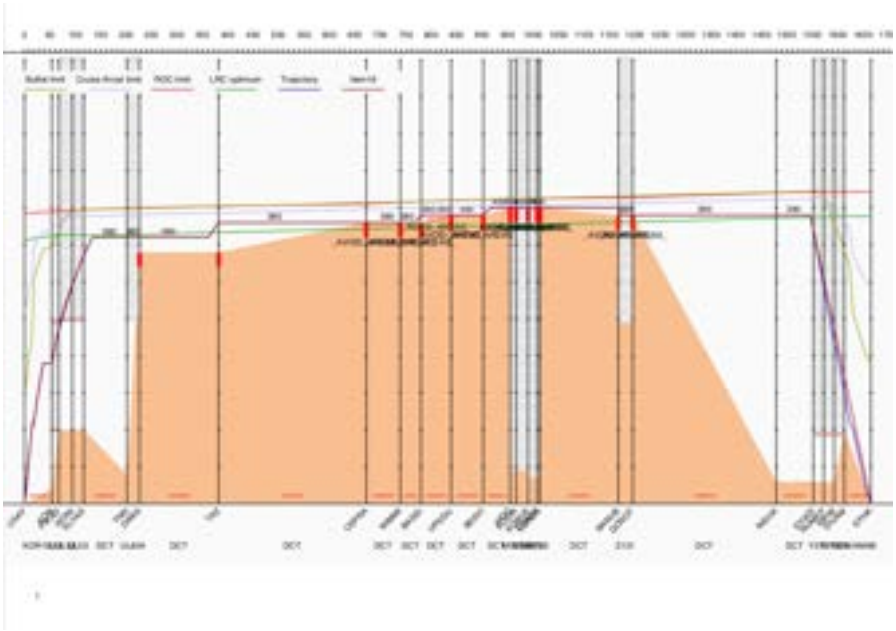

**Figure A.13:** The vertical profile for the LROP-LMML route during a fall night **with** avoidance areas. Note that the trajectory (dark blue) can be hidden by item18 (red).

**Department of Space, Earth and Environmental Science**

**CHALMERS UNIVERSITY OF TECHNOLOGY**
Gothenburg, Sweden
www.chalmers.se


CHALMERS
UNIVERSITY OF TECHNOLOGY